ARTICLES
https://doi.org/10.1038/s41477-020-0605-7

nature plants

Integrated multi-omics framework of the plant response to jasmonic acid

Mark Zander[1,2,3,11], Mathew G. Lewsey[4,5,11]✉, Natalie M. Clark[6], Lingling Yin[4,5], Anna Bartlett[2], J. Paola Saldierna Guzmán[1,9], Elizabeth Hann[1,10], Amber E. Langford[1], Bruce Jow[2,3], Aaron Wise[7], Joseph R. Nery[2], Huaming Chen[2], Ziv Bar-Joseph[7], Justin W. Walley[6], Roberto Solano[8] and Joseph R. Ecker[1,2,3]✉

Understanding the systems-level actions of transcriptional responses to hormones provides insight into how the genome is reprogrammed in response to environmental stimuli. Here, we investigated the signalling pathway of the hormone jasmonic acid (JA), which controls a plethora of critically important processes in plants and is orchestrated by the transcription factor MYC2 and its closest relatives in *Arabidopsis thaliana*. We generated an integrated framework of the response to JA, which spans from the activity of master and secondary regulatory transcription factors, through gene expression outputs and alternative splicing, to protein abundance changes, protein phosphorylation and chromatin remodelling. We integrated time-series transcriptome analysis with (phospho)proteomic data to reconstruct gene regulatory network models. These enabled us to predict previously unknown points of crosstalk of JA to other signalling pathways and to identify new components of the JA regulatory mechanism, which we validated through targeted mutant analysis. These results provide a comprehensive understanding of how a plant hormone remodels cellular functions and plant behaviour, the general principles of which provide a framework for analyses of cross-regulation between other hormone and stress signalling pathways.

Plant hormones are structurally unrelated, small signalling molecules that play pivotal roles in a wide range of fundamental processes of plants, including growth, development and responses to environmental stimuli[1]. Hormone perception by plants stimulates a cascade of transcriptional reprogramming that ultimately modifies cellular function and plant behaviour[2–5]. This is initiated by one or a family of high-affinity receptors, followed by signal transduction through protein–protein interactions, post-translational modification events and regulation of transcription factor (TF) activity that ultimately drive changes in gene expression[2,3,6].

One of the key plant hormones is jasmonic acid (JA), which regulates crucial processes, including fertility, seedling emergence, the response to wounding and the growth–defence balance[7]. Jasmonates are perceived as jasmonoyl-isoleucine by a complex comprising the co-receptors CORONATINE INSENSITIVE1 (COI1) and JASMONATE ZIM DOMAIN (JAZ)[8–11]. COI1 is an F-box protein and part of a Skp–Cullin–F-box E3 ubiquitin ligase complex (SCF^{COI1})[12] that targets JAZ proteins for proteasomal degradation after JA perception. JAZ proteins are transcriptional repressors that inhibit the activity of key TFs of the JA pathway such as the basic helix–loop–helix (bHLH) TF MYC2 and its closest homologues MYC3, MYC4 and MYC5 (refs. [13–15]) in the absence of JA. The SCF^{COI1}–JAZ complex tightly controls the level of free non-repressed MYCs in a JA-dependent manner, thereby determining the transcriptional output of the entire JA response[8,9,16]. The key regulatory step in the JA pathway is the hormone-triggered formation of a complex between the E3 ligase SCF^{COI1} and JAZ repressors that are bound to the master regulatory TF MYC2. This results in the degradation of JAZ repressors and permits the activity of MYC2, accompanied by MYC3, MYC4, MYC5 and numerous other TFs, all of which have distinct but overlapping roles in driving JA-responsive gene expression[13–20]. The result is a cascade of JA-induced genome reprogramming to modulate plant behaviour such as plant immune responses[4,19,21]. However, our knowledge of the JA-responsive genome regulatory programme and, more broadly, in the general response of plants to environmental stimuli is currently limited by assessments of only one or a small number of components.

Here, we aimed to decipher the MYC2–MYC3-driven regulatory network using a multi-omics analysis that includes the direct targets of key TFs, chromatin modifications, global protein abundance and protein phosphorylation. Our analysis was conducted with etiolated seedlings, for which the JA regulatory network is poorly characterized even though MYC2 is active[21–23]. We discovered that MYC2 and MYC3 directly target hundreds of TFs, resulting in a large gene regulatory network that not only amplifies the transcriptional JA response but also facilitates extensive crosstalk with other signalling pathways. Furthermore, we found that MYC2 has a profound impact on the JA-dependent epigenome, proteome and phosphoproteome. We also generated a network model that predicted new components of the JA signalling pathway, which we validated

[1]Plant Biology Laboratory, Salk Institute for Biological Studies, La Jolla, CA, USA. [2]Genomic Analysis Laboratory, Salk Institute for Biological Studies, La Jolla, CA, USA. [3]Howard Hughes Medical Institute, Salk Institute for Biological Studies, La Jolla, CA, USA. [4]Centre for AgriBioscience, Department of Animal, Plant and Soil Sciences, School of Life Sciences, La Trobe University, Melbourne, Victoria, Australia. [5]Australian Research Council Industrial Transformation Research Hub for Medicinal Agriculture, Centre for AgriBioscience, La Trobe University, Bundoora, Victoria, Australia. [6]Plant Pathology and Microbiology, Iowa State University, Ames, IA, USA. [7]Computational Biology Department, School of Computer Science, Carnegie Mellon University, Pittsburgh, PA, USA. [8]Department of Plant Molecular Genetics, Centro Nacional de Biotecnología, Consejo Superior de Investigaciones Científicas (CNB-CSIC), Madrid, Spain. [9]Present address: School of Natural Sciences, University of California Merced, Merced, CA, USA. [10]Present address: Department of Chemical and Environmental Engineering, Department of Botany and Plant Sciences, University of California, Riverside, CA, USA. [11]These authors contributed equally: Mark Zander and Mathew G. Lewsey. ✉e-mail: m.lewsey@latrobe.edu.au; ecker@salk.edu

by targeted genetic analyses, thus demonstrating the power of our integrated multi-omics approach to yield fundamental biological insight into plant hormone responses.

Results

MYC2 and MYC3 target a large proportion of JA-responsive genes. To decipher the JA-governed regulatory network with its high degree of dynamic interconnectivity with other signalling pathways, we applied a multi-omics network approach that comprised five newly generated high-quality large-scale datasets (Fig. 1a,b; Extended Data Figs. 1a–i and 2a–d; Supplementary Tables 1 and 2). MYC2 is the master regulatory TF of JA responses, and plants with a null mutation of this TF have a clear decrease in JA sensitivity[15]. Thus, we included the *myc2* (*jin1-8* SALK_061267) mutant[15] in our analyses (Fig. 1b). MYC2 is responsible for strong JA-responsive gene activation and acts additively with MYC3 and MYC4 (refs. [13,15–20]). *myc3* and *myc4* single mutants behave like wild-type (WT) plants with regards to JA-induced root growth inhibition. However, in combination with the *myc2* mutant, *myc2 myc3* double mutants exhibit an increased JA hyposensitivity, almost as pronounced as in *myc2 myc3 myc4* triple mutants[13]. We consequently selected MYC3 for an in-depth analysis. To better understand how the master TFs MYC2 and MYC3 control the JA-induced transcriptional cascade, we determined their genome-wide binding sites using chromatin immunoprecipitation (ChIP) with sequencing (ChIP-seq). Four biological replicates of JA-treated (2 h) 3-day-old etiolated *Arabidopsis* seedlings that express a native promoter-driven and epitope (YPet)-tagged version of MYC2 and three biological replicates of MYC3 (Col-0 *MYC2::MYC2-YPet*, Col-0 *MYC3::MYC3-YPet*) were used[24]. The rationale behind dissecting jasmonate signalling in etiolated seedlings is that although MYC2 is highly expressed in etiolated seedlings and regulates important processes such as photomorphogenesis and apical hook formation[21–23], a comprehensive characterization of this special developmental stage is still missing.

We identified 6,736 MYC2 and 3,982 MYC3 high-confidence binding sites ($P \leq 1 \times 10^{-25}$ and conserved in at least two independent biological replicates), equating to 6,178 MYC2 and 4,092 MYC3 target genes (within 500 nucleotides of a binding site centre or nearest neighbouring gene) (Fig. 1c,d; Supplementary Table 1). Of the target genes identified, 3,847 were shared, meaning that almost all MYC3 target genes are also bound by MYC2 (Fig. 1c,d). Their target genes were enriched for JA-related gene ontology (GO) terms and for terms related to other hormones (Extended Data Fig. 3a). Target genes shared between MYC2 and MYC3 were significantly enriched ($P < 0.05$) for more JA-related GO terms than for target genes unique to either TF (Extended Data Fig. 3b). Proteins encoded by shared MYC2 and MYC3 target genes were enriched for DNA binding and transcriptional regulatory domains; in contrast, proteins encoded by MYC2-only target genes were enriched for kinase domains (Supplementary Table 3). No significant protein domain or GO term enrichment was detected among the small number of MYC3-only targets (Supplementary Table 3). Collectively, these data indicate that MYC2 and MYC3 have the potential to regulate 23.2% of genes in the *Arabidopsis* genome (27,655 coding genes). However, binding events are not necessarily regulatory[2,3,25]. Using RNA sequencing (RNA-seq), we determined that 2,522 genes were differently expressed (false discovery rate (FDR) < 0.05) after 2 h of JA treatment. One-third (843 genes) of JA-modulated genes were directly bound by MYC2 or MYC3 (Fig. 1d; Supplementary Table 4). This is consistent with the important role of MYC2 and MYC3 in JA-responsive gene expression[13,15–17,19,20]. The majority of JA-responsive genes that are directly targeted by MYC2 and MYC3 were transcriptionally upregulated after JA application, which indicates that MYC2 and MYC3 predominantly act as transcriptional activators (Extended Data Fig. 3c).

The G-box (CA[C/T]GT[G/T]) motif was the most common DNA sequence motif found at MYC2 or MYC3 binding sites, which is concordant with the observation that they shared a large proportion of their binding sites (Fig. 1e,f). This motif was also similar to a motif sequence bound by MYC2 that was determined in vitro[26]. The majority of MYC2 and MYC3 binding sites contained the G-box motif (4,240 out of 6,736 for MYC2, and 3,072 out of 3,982 for MYC3) (Fig. 1e,f; Supplementary Table 5). However, the absence of the motif from a substantial number of MYC2 and MYC3 binding sites suggests that the TFs may bind indirectly to some sites through a partner protein (or proteins). We identified putative partner TFs by determining DNA motifs enriched in MYC2 binding sites that did not contain a G-box motif. The most strongly enriched motifs were CACG[A/C]G (286 sites, statistical significance estimate of a motif (E) = 2×10^{-52}), which may correspond to the TFs CAMTA1 (also known as AT5G09410) or FAR1 (also known as AT4G15090), and AT[A/T][A/T] [A/T]ATA (714 sites, $E = 8.9 \times 10^{-35}$), which may correspond to the ARID family TFs AT2G17410 and AT1G04880 (Extended Data Fig. 3d,e). Molecular investigations of these TFs would be required to determine whether they bind cooperatively with MYC2 to DNA.

Master TFs directly target the majority of signalling components in their respective pathway, a phenomenon that has already been observed for the ethylene, abscisic acid (ABA) and cytokinin signalling pathways[2,3,27]. This pattern also holds true for the JA signalling pathway. Our MYC2 and MYC3 ChIP-seq analyses determined that approximately two-thirds of the genes encoding for known JA pathway components (112 out of 168 genes for MYC2, and 96 out of 168 genes for MYC3) were bound by MYC2 and MYC3 (Extended Data Fig. 4a,b; Supplementary Table 6). Interestingly, the majority of all known JA genes that were differentially expressed following JA treatment were bound by MYC2 or MYC3, whereas fewer non-differentially expressed known JA genes were directly targeted (Extended Data Fig. 4b; Supplementary Table 6). MYCs initiate various feedforward loops that enable rapid activation of the transcriptional JA response[19,28]. Our ChIP-seq approach revealed that beyond the autoregulation of MYC2 and MYC3, these TFs also regulate JA biosynthesis either directly by targeting the JA biosynthesis genes *LOX2*, *LOX3*, *LOX4*, *LOX6* and *AOS* or indirectly through binding to the AP2-ERF TF gene *ORA47* (Supplementary Tables 1 and 6). In addition, MYCs simultaneously target various negative regulators, enabling MYCs to efficiently dampen the JA response pattern (Extended Data Fig. 4c). Key negative regulators of JA signalling are the JAZ repressors, a gene family of 13 members in *Arabidopsis*[29], which can interact with the adaptor protein NINJA to confer TOPLESS-mediated gene repression[30]. Strikingly, all JAZ members and NINJA are directly bound by MYC2 and MYC3 (Extended Data Fig. 4c), which probably leads to a dampening of the JA response and thereby preventing excessive activation of JA signalling.

MYC2 and MYC3 activate the JA response through a large TF network. To study the MYC2 and MYC3-governed transcriptional regulatory network in more detail, we investigated the relationship between MYC2-bound and MYC3-bound TF-encoding genes and their transcriptional responsiveness to JA treatment. We conducted a JA time-course experiment (time points of 0, 0.25, 0.5, 1, 2, 4, 8, 12 and 24 h post JA treatment) and identified a total of 7,377 differentially expressed genes at one or more time points within 24 h of JA treatment (Supplementary Table 4). Differentially expressed genes were categorized into clusters with similar expression trends over time to facilitate the visualization of complex expression dynamics and enriched functional annotations (Extended Data Fig. 5a; Supplementary Table 7). The largest upregulated cluster was the "JA cluster", which was enriched for GO terms associated with JA responses (Fig. 2a). In contrast, the "Cell wall cluster" was the largest cluster of downregulated genes and enriched for GO terms

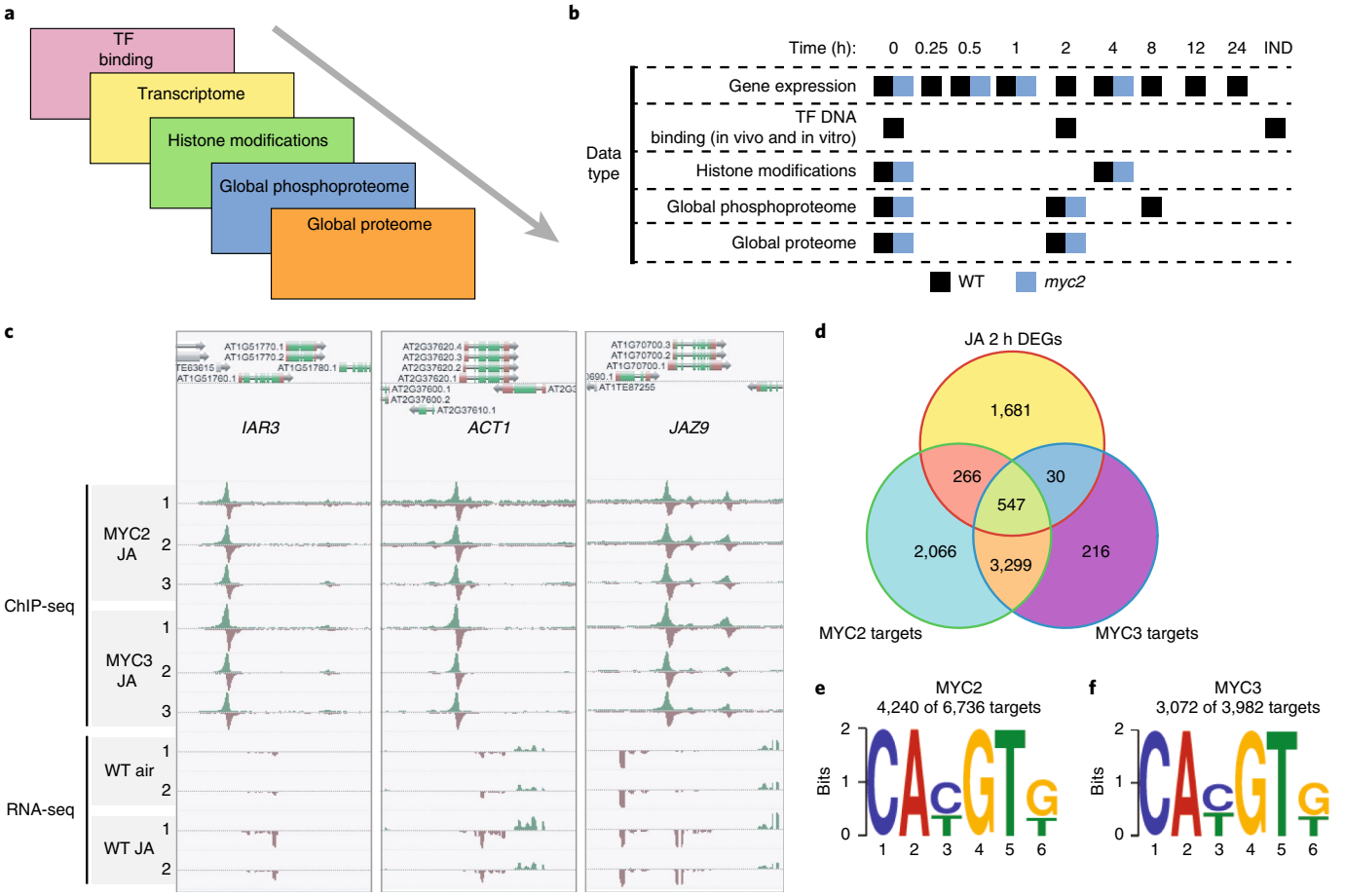

Fig. 1 | Design of our study and key datasets utilized. a,**b**, Overview of profiled regulatory layers (**a**) and detailed description of collected samples (**b**). IND, indefinite. **c**, AnnoJ genome browser screenshot visualizing the binding of MYC2 and MYC3 to three example genes: *IAR3* (also known as JR3), *ACT1* and *JAZ9* (also known as *TIFY7*). MYC2 and MYC3 binding was determined by ChIP-seq using JA-treated (2 h) Col-0 *MYC2::MYC2-YPet* and Col-0 *MYC3::MYC3-YPet* seedlings. Three independent biological ChIP-seq replicates are shown. In addition, mRNA expression of the three example genes and WT seedlings (with or without (that is, air) 2 h of JA treatment) is shown. Expression data were derived from RNA-seq analysis. **d**, Venn diagram illustrating the overlap between MYC2, MYC3 target genes and differentially expressed genes (DEGs) after 2 h of JA treatment (JA 2 h DEGs). **e**,**f**, The top-ranked motif in MYC2 (**e**) and MYC3 (**f**) ChIP-seq data was the G-box (CAC/TGTG) motif. Motifs were determined by MEME analysis using the top-ranked peaks that were identified using the GEM tool.

associated with cell wall organization, development and differentiation (Fig. 2b). These two main clusters illustrate the defence–growth trade-off when defence pathways are activated[31].

Our MYC2 and MYC3 ChIP-seq dataset derived from a 2-h-long JA treatment revealed that up to 63% (0.5 h JA treatment) of differentially expressed genes at any given time point were potentially directly bound by MYC2 and/or MYC3 (Fig. 2c), which highlights the important role of MYCs in transcriptionally regulating JA responses. Our analysis also determined that 522 out of 1,717 known or predicted TFs were differentially expressed within 24 h of JA treatment (Extended Data Fig. 5b). Half of these (268), representing 36 out of 58 TF families, were also direct MYC2 or MYC3 targets (Fig. 2d; Extended Data Fig. 5b), which indicates that MYC2 and MYC3 cooperatively control a massive TF network. The three most numerous families (ERFs, bHLHs and MYBs) in the *Arabidopsis* genome had the most JA-responsive members targeting MYC2 or MYC3, which is concordant with their previously annotated roles in JA responses[32] (Fig. 2d). Plant hormone crosstalk is critical for deploying an appropriate cellular response to environmental stimuli, and numerous reports describe that MYC2 connects the JA pathway to other major plant hormone pathways[23,33]. To investigate this crosstalk function of MYC2 and MYC3 in more detail, we utilized our ChIP-seq data to determine the number of plant hormone TFs that are bound by MYC2 and MYC3. We found that 37–59% of annotated hormone pathway genes are bound by MYC2 and MYC3 and that their expression changes in response to 24 h of JA treatment (Extended Data Fig. 5c). In addition, we discovered 122 annotated hormone TFs, with representatives from all hormone pathways, that are bound by MYC2 and MYC3, and 118 of these were differentially expressed (Extended Data Fig. 5d; Supplementary Table 1).

We next set out to better understand the target genes of the network of TFs downstream of MYC2 and MYC3. To do so we conducted ChIP-seq or DNA affinity purification (DAP) with sequencing (DAP-seq) on a subset of TFs ((DREB2B (also known as AT3G11020), ATAF2, HY5 (also known as AT5G11260), RVE2 (also known as AT5G37260) and ZAT18 (also known as AT3G53600)) that were direct MYC2 or MYC3 targets and rapidly upregulated (within 0.5 h) by JA treatment (Fig. 2e) or were members of the upregulated "JA cluster" (TCP23 (also known as AT1G35560) (Fig. 2a). We also included the following TFs with known roles in JA signalling: ERF1 (also known as AT3G23240, ERF1B and AtERF092); ORA59 (also known as AT1G06160); ANAC055 (also known as NAC3); WRKY51 (also known as AT5G64810); and STZ (also known as ZAT10)[34–38]. These TFs formed a highly connected network, with all TFs except

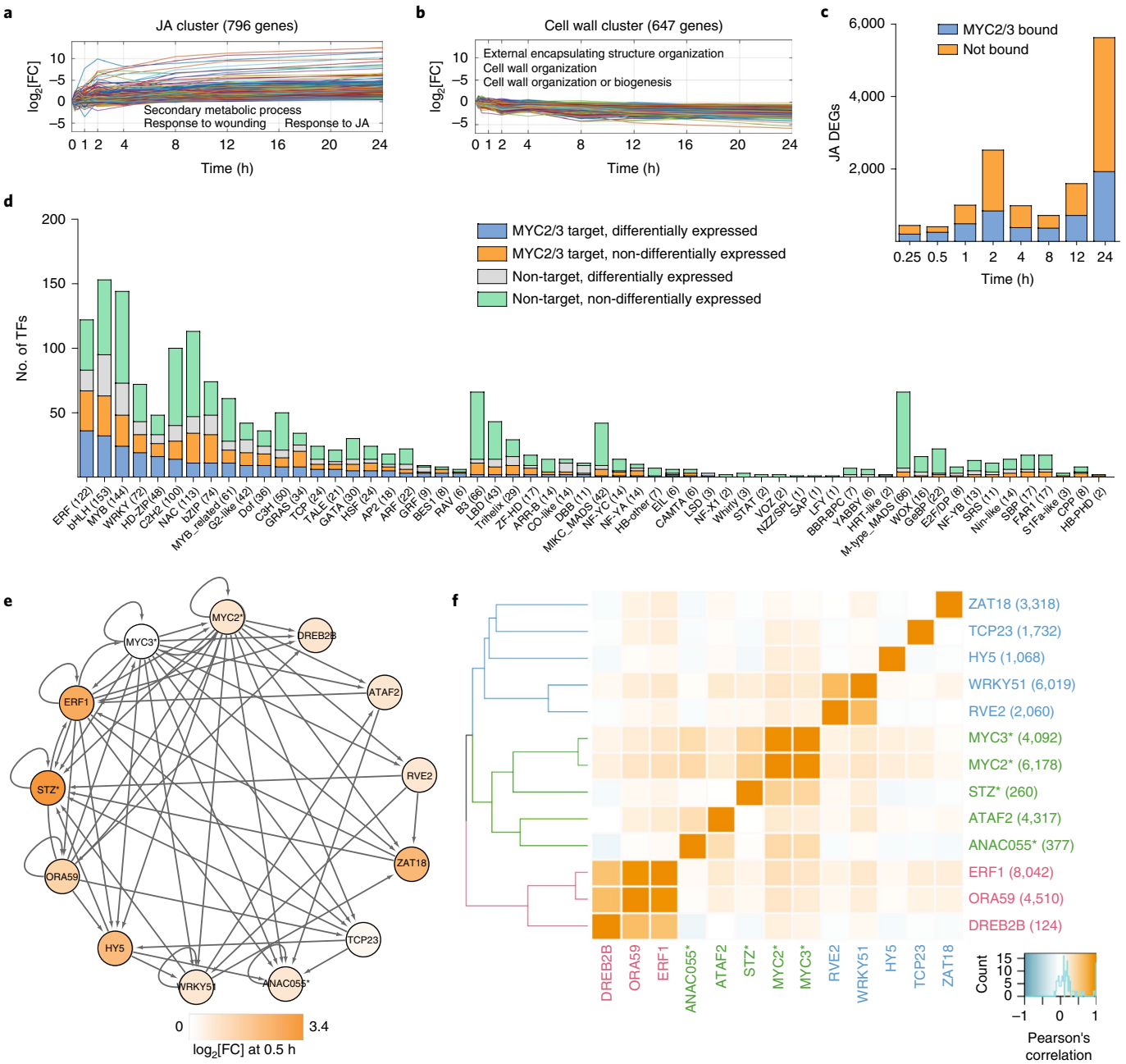

Fig. 2 | MYC2 and MYC3 target a large proportion of JA-responsive genes that encode TFs. a,**b**, A cluster analysis revealed two main clusters in the JA time-course experiment. The JA cluster (**a**), with 796 genes, reflects the majority of JA-induced genes and the cell wall cluster (**b**), with 647 genes, represents the largest cluster of JA-repressed genes. Clusters visualize the $\log_2$ fold-change ($\log_2$[FC]) expression dynamics over the indicated 24-h time period. The three strongest enriched GO terms for each cluster are also shown. Clusters were identified by STEM clustering (Pearson's correlation, minimum correlation of 0.7, and up to 50 permutations; significant clusters were Bonferroni-corrected at $P < 0.05$). For each of the indicated time points, the expression of three independent samples ($n = 3$) was measured using RNA-seq. **c**, Bar plots illustrating the potential of MYC2 and/or MYC3 (MYC2/3) to bind to a portion of JA DEGs at the indicated time points. JA DEGs for all time points were identified by RNA-seq. MYC2 and MYC3 targets were derived from ChIP-seq analysis using Col-0 *MYC2::MYC2-YPet* and Col-0 *MYC3::MYC3-YPet* seedlings that were treated for 2 h with JA. **d**, MYC2 and MYC3 target genes from a wide range of TF families. TF families are classified into the following four different groups: MYC2 and MYC3 targets and differentially expressed after JA treatment; MYC2 and MYC3 targets and not differentially expressed; not bound by MYC2 or MYC3 but differentially expressed; and not bound by MYC2 or MYC3 but not differentially expressed. **e**, Nodes represent JA TFs for which direct binding data were generated. ChIP-seq data are indicated by asterisks; all other data are DAP-seq. Edges represent binding events and are directed. Self-loops indicate that the TF binds to its own locus, which is indicative of potential autoregulation. Expression of the TF at 0.5 h after JA treatment is represented by the coloured scale. **f**, Pearson's correlation of TF target sets of genes. Numerals in parentheses indicate the total number of target genes. ChIP-seq data are indicated by asterisks, all other data were generated by DAP-seq. ChIP-seq data were derived from at least three independent experiments: MYC2 (JA, $n = 4$), MYC3 (JA, $n = 3$), STZ (air, $n = 3$; JA, $n = 2$), ANAC055 (JA, $n = 3$). DAP-seq data were derived from a single experiment ($n = 1$).

DREB2B targeting at least two TFs in the network and these two in turn targeted by two TFs (Fig. 2e; Supplementary Table 8). Autoregulation was common, with seven TFs targeting their own loci (Fig. 2e). The target genes of STZ, ANAC055 and ATAF2 were most similar to those of MYC2 and MYC3 (Fig. 2f). Consistent with this, their target genes shared several significantly enriched GO terms (adjusted $P < 0.05$), which suggests that there are related functions in jasmonate signalling (Extended Data Fig. 6a). ORA59 and ERF1, along with DREB2B, formed a distinct group that targeted a related set of genes (Extended Data Fig. 6a). Notably, ERF1 and ORA59 also shared significant enrichment of a separate set of GO terms with one another, but these were not enriched among MYC2 and MYC3 targets (Extended Data Fig. 6a). This is consistent with the joint role of ERF1 and ORA59 in controlling a pathogen defence arm of JA signalling[34,35]. No GO terms were enriched among the targets of DREB2B. WRKY51 and RVE2 had relatively few enriched GO terms but shared most of these with one another (Extended Data Fig. 6a). Most of the terms related to anti-insect defence and were a subset of the enriched MYC2 and MCY3–STZ–ANAC055–ATAF2 GO terms (Extended Data Fig. 6a). STZ and ANAC055 are known regulators of anti-insect defence and our results suggest that WRKY51 and RVE2 may also be involved in this component of jasmonate responses[39]. Interestingly, *STZ* belongs to a group of genes that is inducible by the JA precursor 12-oxo-phytodienoic acid (OPDA) and not by JA[40]. We found that approximately one-third of OPDA-specific response genes (45 genes) are targeted by MYC2 (Supplementary Table 3). Taken together, our analyses determine that MYC2 and MYC3 shape the dynamic JA response through the activation of a large TF network that includes various potentially coupled feedforward and feedback loops and allows extensive cross-communication with other signalling pathways.

We examined the effect of removing MYC2 activity on JA-responsive transcriptional regulation by generating transcriptomes from a *myc2* null mutant (*jin1-8*) in an early JA response time-series experiment (0, 0.5, 1 and 4 h). The response of *myc2* mutants to JA differed from that of WT plants. There were 2,905 unique genes differentially expressed between *myc2* and WT plants across the time-series (pairwise comparisons between genotypes at each time point; Supplementary Table 9). JA-responsive gene expression occurred in *myc2* plants, which is consistent with the partially redundant function of MYC2, MYC3 and MYC4 (ref. [13]). However, JA-responsive genes were upregulated more highly in WT than *myc2* plants (Supplementary Table 9). The *JAZ* genes illustrate this, with 9 out of the 12 genes upregulated more highly in WT than *myc2* plants, as well as reaching peak expression at earlier time points in WT plants (0.5 or 1 h; (Extended Data Fig. 7a). Overall, a majority of the MYC2 target genes differentially expressed between *myc2* and WT plants were more highly expressed in WT, which indicates that loss of MYC2 function reduces the JA responsiveness of these genes (Extended Data Fig. 7b). A total of 130 TFs targeted by MYC2 were differentially expressed in *myc2* mutants compared with WT seedlings, including the TFs ATAF2, ERF1, ANAC055 and STZ, whose targets we had determined by DAP-seq or ChIP-seq (Supplementary Table 10). The *myc2* mutation also affected the expression of secondary, indirect MYC2 target genes (that is, genes targeted by MYC2-regulated TFs, but not by MYC2 itself). Between 23.6% and 26.3% of the genes each targeted by ATAF2, ERF1, ANAC055 or STZ, and not by MYC2, were differentially expressed in *myc2* plants compared with WT (Extended Data Fig. 7c; Supplementary Table 11). Taken together, these data demonstrate that MYC2 regulates gene expression through a large network of downstream TFs during responses to a JA stimulus.

MYC2 controls JA-induced epigenomic reprogramming. Reprogramming of the epigenome is an integral part of development and environmental stimulus-induced gene expression[41]. For example, activation of the transcriptional JA response requires the formation of MYC2–MED25-mediated chromatin looping[42]. To investigate the extent of JA-induced changes in chromatin architecture and the regulatory importance of MYC2 in this response, we conducted ChIP-seq assays to profile the genome-wide occupancy of the histone modification H3K4me3 (trimethylation of lysine 4 on histone H3) and the histone variant H2A.Z in untreated and in JA-treated (4 h) WT and *myc2* seedlings. H3K4me3 marks active and poised genes whereas the histone variant H2A.Z confers gene responsiveness to environmental stimuli[43,44]. mRNA expression was monitored in parallel using RNA-seq. JA treatment led to a reprogrammed chromatin landscape, with several thousand differentially enriched H3K4me3 and H2A.Z domains (Extended Data Fig. 8a–c; Supplementary Table 12). We identified 826 differentially expressed genes (675 induced, 151 repressed; WT control versus JA treated) in that experiment. In line with the predominantly activating function of MYC2 (Extended Data Fig. 3c), the JA-induced genes had a stronger promoter enrichment of MYC2 than the JA-repressed genes (Fig. 3a). H3K4me3 levels were increased in JA-induced genes, whereas JA-repressed genes did not exhibit any dynamic change in H3K4me3 levels (Fig. 3b,d). Strikingly, *myc2* mutants only displayed a compromised increase in H3K4me3 levels after JA treatment, which suggests that the JA-induced H3K4me3 depends on functional MYC2 (Fig. 3b–d; Extended Data Fig. 8a). The impact of the *myc2* mutation on JA-induced H3K4me3 changes were also observed in JA-induced genes that are not directly targeted by MYC2 (Extended Data Fig. 8e,f), which is potentially caused by the decreased expression of MYC2-targeted TFs. The scenario of a direct MYC2 regulation network is illustrated by two JA-induced genes, *JAZ2* and *GRX480*, which are directly targeted by MYC2. Their expression depends on MYC2, and their JA-induced increase in gene-body-localized H3K4me3 partially depended on MYC2 (Fig. 3d; Extended Data Fig. 8d). However, whether the MYC2-dependent changes in H3K4me3 levels precede transcription or rather reflect increased transcriptional activity cannot be addressed by these experiments. In contrast, JA-induced changes in H2A.Z occupancy were only slightly affected in *myc2* mutants (Extended Data Fig. 8a,g,h), which suggests that JA-induced H2A.Z dynamics are either independent of MYC2 or precede MYC2 binding. Alternatively, other MYCs such as MYC3, MYC4 and MYC5 are functionally redundant in regulating H2A.Z dynamics.

JA extensively remodels the (phospho)proteome. We next explored how JA remodels the proteome and phosphoproteome of etiolated seedlings. Hormone signal transduction typically modifies the phosphorylation of downstream proteins, changing their activity independent of transcript abundance[6]. Transcript abundance is also frequently weakly correlated with protein abundance[45,46]. Consequently, proteomic and phosphoproteomic analyses yield additional insight into gene regulatory networks. We determined that the loss of MYC2 caused substantial changes to the JA-responsive proteome and phosphoproteome; 1,432 proteins and 939 phosphopeptides (corresponding to 567 genes) were significantly differentially abundant in WT seedlings relative to *myc2* seedlings after 2 h of JA treatment ($q < 0.1$; Fig. 4a; Supplementary Tables 13 and 14). WT seedlings responded to JA (161 proteins, 443 phosphopeptides, WT JA versus WT air), and the response was smaller without functional MYC2 (79 proteins, 93 phosphopeptides, *myc2* JA versus *myc2* air) (Fig. 4a). These extensive changes in phosphopeptide abundance are consistent with the observation that 118 genes encoding protein kinases were differentially expressed between WT and *myc2* seedlings in our transcriptome experiments (Supplementary Table 9).

Some direct overlap existed between proteins or phosphopeptides and transcripts responsive to JA treatment (Fig. 4b). Both transcripts and proteins encoded by 28 genes were differentially

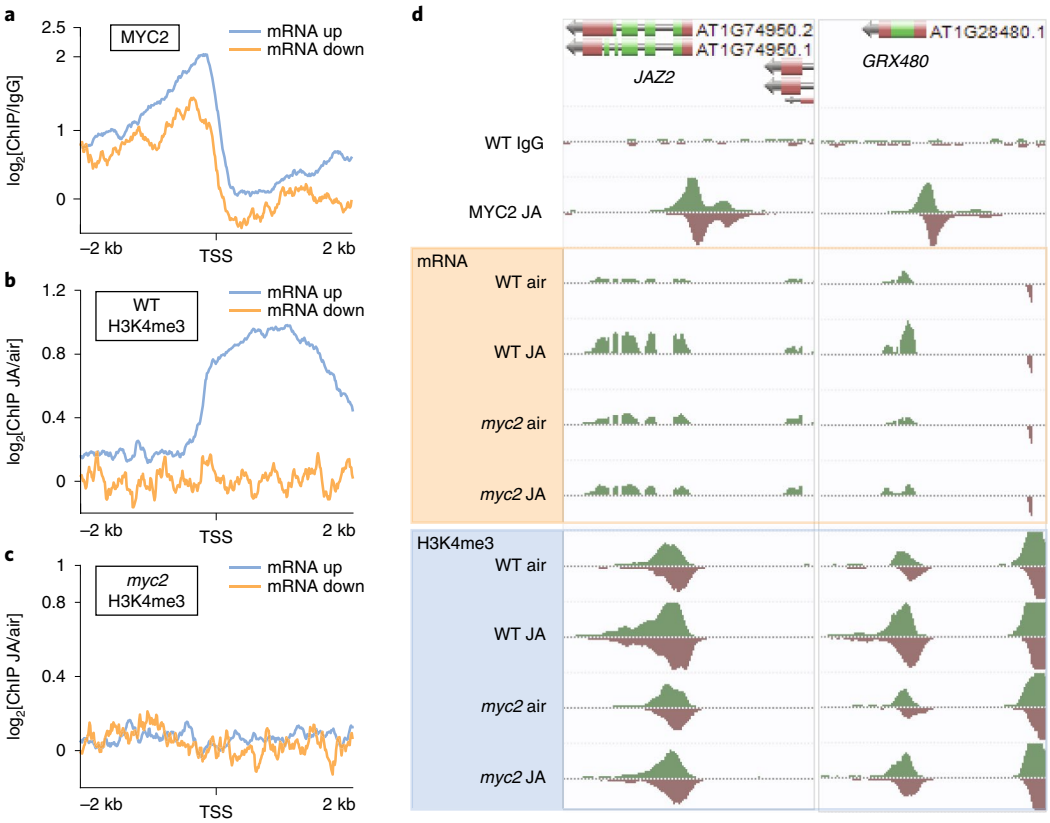

Fig. 3 | The JA-responsive epigenome. a–c, Aggregated profiles showing the $\log_2$[FC] enrichment of MYC2 (**a**), H3K4me3 WT (**b**) and H3K4me3 *myc2* (**c**) from 2-kb upstream to 2-kb downstream of the transcriptional start site (TSS) at JA-induced and JA-repressed genes. The profile of MYC2 is shown for Col-0 *MYC2::MYC2-YPet* seedlings (**a**) and H3K4me3 profiles are shown are shown for WT (**b**) and *myc2* (**c**) seedlings. **d**, AnnoJ genome browser screenshot visualizing MYC2 binding, mRNA expression and H3K4me3 occupancy at two example genes (*JAZ2* and *GRX480*) in WT and *myc2* seedlings. All tracks were normalized to the respective sequencing depth.

expressed in JA-treated WT seedlings relative to air controls (Fig. 4b). A further 33 differentially expressed proteins in JA-treated WT seedlings had no corresponding differentially expressed transcript, but were encoded by genes that are targeted by MYC2 and MYC3 (Fig. 4b). Differentially abundant phosphopeptides were detected that corresponded to 15 differentially expressed transcripts (Fig. 4b). Transcript and protein abundance was weakly positively correlated (Pearson's correlation value of 0.40341) in JA-treated WT seedlings (Fig. 4c), which is in agreement with previous studies[45,46]. The protein of only one known JA pathway component was differentially abundant in JA-treated WT seedlings relative to controls, and none were differentially phosphorylated. The fact that only a single JA-regulated protein and no phosphoproteins were annotated as JA pathway components may indicate that existing annotations are overly dependent on transcriptome data and that consideration of (phospho)proteome data deepens our understanding of JA responses.

Alternative splicing can rapidly occur in response to environmental stimuli, contributing to transcriptome reprogramming and potentially fine-tuning physiological responses[47]. It is central to the JA-mediated regulation of transcription, with an alternative isoform of the repressor JAZ10 creating a negative feedback loop that desensitizes cells to a JA stimulus[48,49]. However, the extent of alternative splicing in JA signalling beyond the JAZ repressors is poorly characterized. We observed that phosphorylation of proteins involved in RNA recognition and nucleotide binding was disrupted in JA-treated *myc2* mutants compared with WT seedlings. The spliceosome was the only pathway significantly enriched among these differentially phosphorylated proteins ($P < 0.05$, 18 genes matched), which suggests that MYC2 may influence JA-responsive alternative splicing. Furthermore, 18 genes with splicing-related annotations were differentially expressed between *myc2* and WT seedlings in our transcriptome experiments (Supplementary Table 9). None of the differentially phosphorylated spliceosome components was differentially expressed.

We examined isoform-switch events across our JA transcriptome time-series, for which the most abundant of two isoforms from a single gene changes, to determine the extent of JA-responsive alternative splicing (Fig. 4d,e; Supplementary Table 15). There were 151 switch events, corresponding to 137 isoform pairs from 120 genes, within 24 h of JA treatment. These were identified from 30,547 total individual transcripts detected (average transcript per million (TPM) > 1; Supplementary Table 16). Two of the genes exhibiting isoform switches had prior JA annotations (*RVE8* (also known as *AT3G09600*) and *SEN1* (also known as *AT4G35770*); Supplementary Table 15), and others were annotated to a variety of processes (including auxin, ABA, light signalling, disease response, among many others), but there was no significant enrichment of any GO terms or pathways. This indicates that MYC2 influences alternative splicing that diversifies the transcriptome in response to a JA stimulus.

Multi-omics modelling of the JA-response regulatory programme. We then wanted to characterize the broader JA-response genome regulatory programme so that we could increase our understanding of the roles of known JA TFs within this and to identify new potential regulatory interactions. To do so, we generated a gene regulatory network model encompassing the

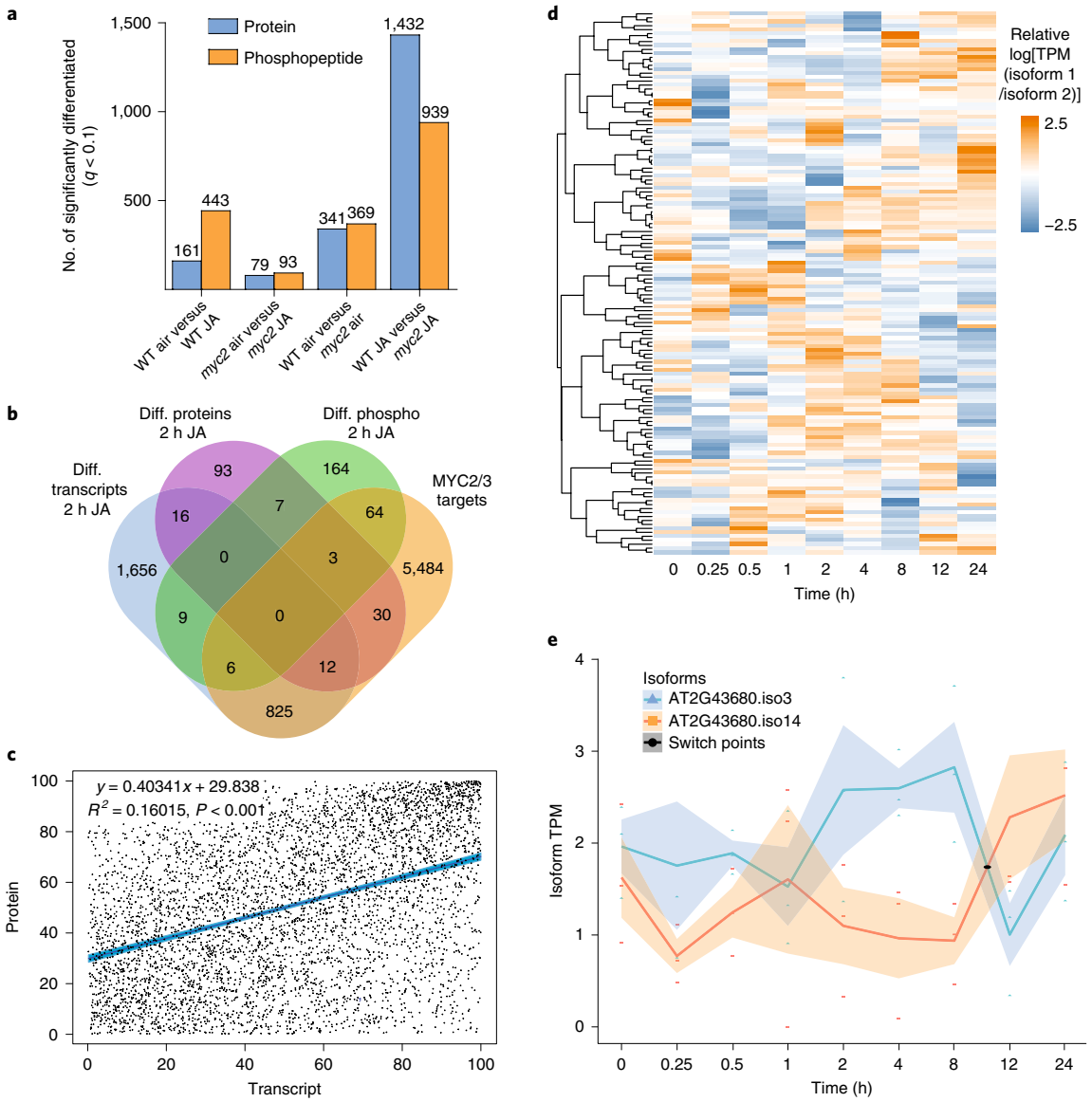

Fig. 4 | Loss of functional MYC2 affects the global proteome and phosphoproteome. a, Total number of significantly differentially abundant (FDR $q < 0.1$; estimated using a modified permutation plug-in method) proteins and phosphopeptides detected in comparisons between JA-treated (2 h) WT and *myc2* seedlings and air controls. Three independent experiments (with or without 2 h of JA treatment; $n = 3$) were conducted for WT and *myc2* seedlings. For the third experiment, only the JA treatment was conducted. **b**, Venn diagram showing the overlap between significantly differentially (Diff.) abundant proteins, transcripts and differentially phosphorylated proteins (Diff. phospho) in JA-treated WT seedlings compared with mock-treated WT controls. Also shown is the overlap with MYC2/3 target genes. **c**, Correlation between rank-normalized $\log_2$ fragments per kilobase of transcript per million (FPKM) values of detected proteins and transcripts in WT seedlings treated with JA for 2 h (*P* value cut-off was <0.05 using paired Student's *t*-tests). Scatter plot of $\log_2$[FC] in WT JA-regulated transcript levels versus $\log_2$[FC] in levels of corresponding proteins. Protein and transcript data were derived from three independent experiments ($n = 3$) using WT and *myc2* seedlings. **d**, Heatmap representing the relative TPM of 137 isoform pairs exhibiting isoform-switch events. Ratio calculated as log[TPM (isoform 1/isoform 2)]. **e**, Plot showing an example of a transcript pair originating from *AT2G43680* that had isoform-switch events following JA treatment. Expression data were derived from a JA time-course experiment. For each of the indicated time points, the expression of three independent samples ($n = 3$) was measured using RNA-seq. Lines indicate the mean TPM of three independent samples. Shaded regions indicate the standard error of these data.

(phospho)proteomic and time-series transcriptomics data (Extended Data Fig. 9a; Supplementary Table 17). Inclusion of the (phospho)proteomic data expanded the network by an additional 957 nodes (genes) compared with a transcript-only network (3,409 versus 4,366 nodes, 28% larger)(Supplementary Table 17). The (phospho)proteomics and transcript data shared 217 nodes within the network, a relatively small proportion, which indicates that these datasets complement one another when attempting to characterize the JA-response genome regulatory programme.

Many known JA signalling components were present in the 100 most important predicted components of the network (for example, MYC2, ERF1, JAZ1, JAZ2, JAZ5, JAZ10 and ATAF2, among others, within the top 100 of 4,366 components assessed using a normalized motif score) (Supplementary Table 17). MYC2 was predicted to regulate a subnetwork of 26 components, 23 of which were validated as directly bound by MYC2 in ChIP-seq assays (88.5%; Extended Data Fig. 10a; Supplementary Tables 1 and 17). We further validated the network by comparing the ChIP-seq and DAP-seq data

previously collected for the remaining 12 JA TFs to their targets in the gene regulatory network (Fig. 2e,f; Extended Data Fig. 10b; Supplementary Table 18). The gene regulatory network identified all of these TFs as components of the JA response, except MYC3 (Supplementary Table 17). It is probable that MYC3 was not considered part of the network because it was only modestly differentially expressed following JA treatment and was not detected in the (phospho)proteome analyses (Supplementary Tables 4, 13 and 14). The wider validation of targets was less strong than for MYC2, ranging from 0% to 33.3%. This could reflect the possibility that interactions predicted by the gene regulatory network may not identify all intermediate components. Last, we examined known genetic interactions. The MYC2 subnetwork included activation of JAZ10 within 0.5 h of a JA stimulus, with JAZ10 reciprocally repressing MYC2 (Extended Data Fig. 10a,b). This is consistent with the known role of JAZ10 in establishing negative feedback to attenuate JA signalling[49]. MYC2 was also predicted to activate ABA-INDUCIBLE BHLH-TYPE TRANSCRIPTION FACTOR (AIB; also known as JAM1, bHLH017 and AT2G46510) (Extended Data Fig. 10a,b), which establishes a negative feedback loop in which AIB negatively regulates MYC2. This is in line with previous studies, which established that AIB is dependent on and antagonistic to MYC2, thereby repressing JA signalling[50,51]. Confirmation by both genetic data from the literature and our DAP-seq and ChIP-seq experiments indicates that our gene regulatory network modelling approach is a useful tool to identify new regulatory interactions within JA signalling and to better understand known regulatory interactions.

Crosstalk between hormone response pathways permits fine-tuning of plant growth and development in response to diverse environmental signals[1]. We examined the potential points at which MYC2 may interface directly with other hormone signalling pathways, since MYC2 is the master regulator of JA responses and one of the first TFs activated by JA. The MYC2 subnetwork identified a potential route for JA signalling to cross-regulate auxin hormone signalling. MYC2 activated ARF18, and ARF18 reciprocally activated MYC2 (Extended Data Fig. 10a; Supplementary Table 17). It also indicated that MYC2 may promote ethylene signalling by activating MAP kinase kinase 9 (MKK9) (Extended Data Fig. 10a). Previous genetic studies have determined that MKK9 induces ethylene production, but had not examined a possible link with JA signalling[52]. Positive crosstalk exists between JA and auxin signalling; however, the mechanism is not clearly determined[53]. RGL3, a regulator of gibberellic acid (GA) signalling previously associated with JA–GA crosstalk[54], was also present within the MYC2 subnetwork (Extended Data Fig. 10a) and predicted to inhibit MYC2 but not to be reciprocally regulated by MYC2. These three interactions are potential points at which crosstalk can rapidly occur during a JA response with auxin, gibberellin and ethylene.

We next examined the broader gene regulatory network to identify additional predicted points of crosstalk between JA and other signalling pathways. The model predicted that STZ is a key early hub through which JA signalling is prioritized over several other hormone and stress response pathways (Fig. 5a; Supplementary Table 17). Genetic studies have shown that STZ is a transcriptional repressor[55], and, consistent with this, our model predicted that it inhibited the majority of genes it regulates (25 out of 34 genes). *WRKY40*, *WRKY70*, *DDF* and *ERF6* were all predicted to be inhibited by STZ within 0.25 h of a JA stimulus and *GRX480* within 1 h. Direct binding of STZ to ERF6 was detected in ChIP-seq assays (Supplementary Table 11). WRKY40 and WRKY70 are both early brassinosteroid response components that repress defence responses[56]. DDF1 promotes resistance to drought, cold, heat and salinity stress by reducing endogenous gibberellin abundance[57]. ERF6 similarly promotes drought resistance by reducing gibberellin abundance[58]. GRX480 regulates the negative crosstalk between salicylic acid and both JA and ethylene signalling through direct interactions with TGA TFs[59,60]. The model also predicted that ERF6, WRKY70 and DDF1 exert negative feedback on STZ by activating JAZ8 within 0.25 h of the JA stimulus (Fig. 5a; Supplementary Table 17). JAZ8 is a repressor of JA signalling and is predicted to repress STZ[61]. In summary, the gene regulatory network predicts that STZ is an important hub for JA signalling to be prioritized over other hormone and stress response pathways (Fig. 5a).

Large-scale data-mediated identification of new JA regulators. We next utilized our regulatory network and large-scale datasets to identify novel regulators of the JA pathway using the JA root-growth inhibition assay as our experimental readout. First, we focused on ABA overly sensitive 3 (ABO3), which is directly targeted by MYC2 and MYC3 (Supplementary Table 1) and whose subnetwork is composed of 26 predicted regulated genes, the majority of which are positively regulated (22 out of 26 genes; Fig. 5b). *ABO3* encodes the *Arabidopsis* WRKY TF gene *WRKY63*, which is involved in stress gene expression and drought tolerance[62]. To investigate the importance of the ABO3 subnetwork in JA signalling, we tested *abo3* T-DNA mutant seedlings (SALK_075986C[63]) in a JA-induced root-growth inhibition assay. We found that *abo3* mutants show a weak JA hyposensitive root-growth inhibition phenotype (Fig. 5c–e), which indicates that ABO3 is positive regulator of JA signalling and that our network approach is able to identify new pathway components.

Next, we expanded our phenotyping analysis to T-DNA lines of genes that display the strongest binding of MYC2 and MYC3 in their promoters (Supplementary Tables 1 and 18). The rationale behind this approach is that master TFs target the majority of key signalling components in their regulated respective pathways and that these are often the most strongly bound targets[2,3,27]. Of the 99 genes tested (194 T-DNA lines in total; Supplementary Table 19), we discovered six genes that, when mutated, display mild JA root-growth phenotypes (Extended Data Fig. 10c; Supplementary Table 19). Mild phenotypes and their low frequency were not surprising, since gene redundancy is very common in the *Arabidopsis* genome, and even the mutation of the master TF MYC2 only causes a mild JA hyposensitive root-growth phenotype[15] (Fig. 5c–e). Among these genes was the cytochrome P450 enzyme *CYP708A2* gene, from which both tested T-DNA mutant alleles exhibited a JA hypersensitive root phenotype (Fig. 5f–h). Interestingly, our network analysis also discovered CYP708A2 as a regulatory hub (Extended Data Figs. 9a and 10d). CYP708A2 is involved in triterpene synthesis, which is stimulated by JA[64]; future studies are, however, needed to further decipher the role of CYP708A2 in JA signalling. Another interesting uncharacterized gene that we discovered to cause a JA phenotype is a Sec14p-like phosphatidylinositol transfer family protein (*AT5G47730*; Extended Data Fig. 10c; Supplementary Table 19). Phosphatidylinositol transfer proteins are crucial for maintaining phosphatidylinositol homeostasis in plants[65], and inositol polyphosphates are implicated in COI1-mediated JA perception[66]. Taken together, these data show that our multi-omics approach goes beyond network description, ultimately enabling the identification of novel JA pathway regulators.

Discussion

An important unanswered question in plant biology is how multiple signalling pathways interact to coordinate the control of growth and development. In this study, we comprehensively characterized cellular responses to the plant hormone JA and generated a network-level understanding of the MYC2 and MYC3-regulated JA signalling pathway. We used this approach to identify several new points at which JA signalling may have cross-regulation with other hormone and stress response pathways to prioritize itself. The results increase our knowledge of how JA functions in the etiolated seedling, a less well-characterized model of JA responses. Moreover, the general principles described here provide a framework for analyses of

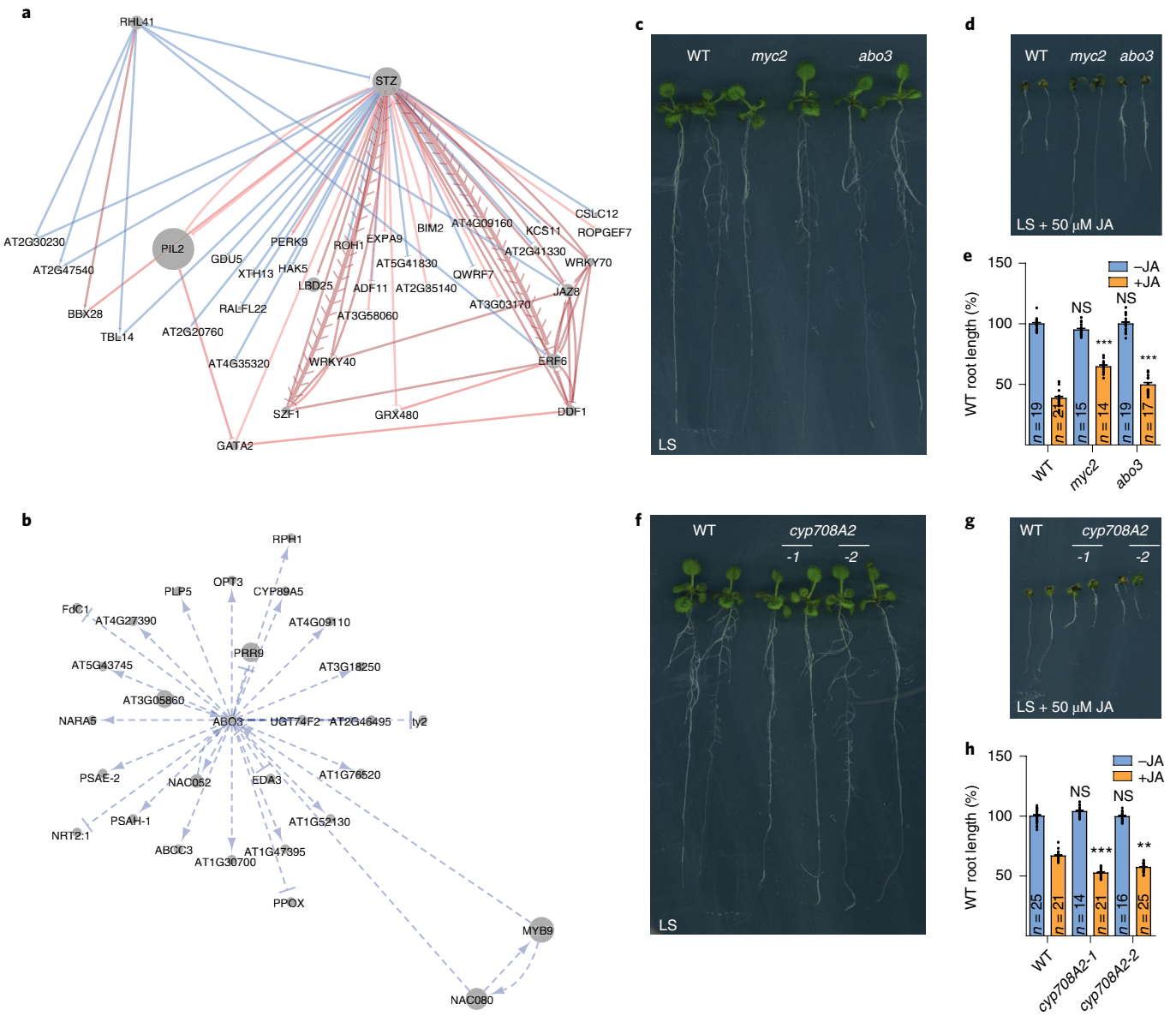

Fig. 5 | JA-response genome regulatory model positions: known and new components. a,**b**, Subnetworks of STZ (**a**) and ABO3 (**b**). Edges are directed. Red edges exist at early time points (0.25–2 h), blue only at late time points (4–24 h). Thicker edges with chevrons indicate that MYC2 directly bound that gene in ChIP-seq experiments. **c**,**d**, JA-induced root-growth inhibition assays identified ABO3 as a positive JA regulator. Seedlings were grown on LS media without (**c**) or with (**d**) 50 µM JA. WT and *myc2* seedlings served as controls. **e**, Quantification (±s.e.m.) of JA-induced root-growth inhibition in WT, *myc2* and *abo3* seedlings. Sample size number (*n*) is shown within the respective bars. Data were derived from three independent experiments. Asterisks represent significant differences between WT (with (+) or without (–) JA treatment) and *abo3* mutants (with or without JA treatment); two-way analysis of variance with Bonferroni post-test, $***P < 0.001$, NS, not significant. **f**,**g**, Root-growth inhibition assays identified two *cyp708A2* T-DNA alleles as JA hypersensitive. Seedlings were grown on LS media without (**f**) or with (**g**) 50 µM JA, and WT seedlings served as controls. **h**, Quantification (±s.e.m.) of JA-induced root-growth inhibition in WT and *cyp708A2* seedlings. Sample size number is shown within the respective bars. Date were derived from three independent experiments. Asterisks represent significant differences between WT (with or without JA treatment) and *cyp708A2* (with or without JA treatment) seedlings. Significant differences were determined using two-way analysis of variance with Bonferroni post-hoc test; $**P < 0.01$, $***P < 0.001$.

cross-regulation between hormone and stress signalling pathways. We provide our data in a web-based genome and in network browsers to encourage deeper exploration (http://signal.salk.edu/interactome/JA.php and http://neomorph.salk.edu/MYC2).

A major insight provided by our study is that multiple points of crosstalk probably exist between JA signalling and other pathways. This was evident from the interactions within the genome regulatory network model and supported by our observation that many (37–59%) genes from other hormone signalling pathways are bound by MYC2 and MYC3 and are regulated by JA. The WRKY family TF ABO3 was identified as a candidate JA response regulator, and genetic analyses determined a mutant of the gene was JA hyposensitive. ABO3 is also a regulator of ABA responses[62], which suggests that ABO3 functions in cross-communication between the JA and ABA pathway. The repressive zinc-finger family TF STZ, working with JAZ8, emerged as a potentially important point of contact with salt and drought stress, as well as the salicylic acid, brassinosteroid and gibberellin hormone signalling pathways. Combined, these

results illustrate the importance of transcriptional cross-regulation during a JA response in modulating the correct cellular output for the stimuli a plant perceives.

Our multi-omics analysis determined that the master TF MYC2 and its relative MYC3 directly target thousands of JA-responsive genes, including hundreds of JA-responsive TFs, thereby enabling a robust cascade of transcriptional reprogramming. Secondary TFs downstream of MYC2 and MYC3 directly targeted overlapping but distinct cohorts of genes, indicating that they have distinct roles within the JA response. This illustrates the complexity of hormone-response genome regulatory programmes; we assayed only a fraction of the JA-responsive TFs and found that any individual JA-responsive gene may be bound by multiple TFs. How the final quantitative output of any individual gene is determined by combinatorial binding of TFs remains a major challenge to address. Achieving this will require analyses at cell-type resolution, resolving differences in TF activity between tissues that would be obscured by our bulk-tissue analyses. We further demonstrated the importance of MYC2 and MYC3 target genes in JA responses by analysing JA root-growth phenotypes in mutants of 99 genes strongly targeted by MYC2 or MYC3. Mutations in six genes caused clear disruptions in JA responses, both hypersensitivity and hyposensitivity. It is probable that genetic redundancy accounts for a proportion of the mutants not causing phenotype changes. The structure of hormone-response genome regulatory programmes will probably differ between cells and tissues and, while our findings can be translated between etiolated seedlings and seedlings grown in light, exploration of other developmental stage-specific regulatory programmes is needed to generalize these findings.

Our study also highlighted that many different regulatory mechanisms are utilized by JA to exert its effects on the cell. Expression of a large number of protein kinases was regulated by MYC2. Consistent with this, substantial MYC2-dependent changes in phosphopeptide abundance occurred in JA-treated seedlings. It is also probable that JA modulates alternative splicing through MYC2. Genes encoding splicing factors were differentially expressed between *myc2* and WT plants, and the spliceosome pathway was enriched among *myc2*-dependent JA-regulated phosphopeptides. Accordingly, isoform-switch events occurred following JA treatment. Collectively, these findings indicate that investigation of post-transcriptional and post-translational layers of regulation are required to better understand the complexity of JA signalling. The targets of JA-regulated protein kinases are a notable prospect.

Another layer of regulatory complexity within the JA signalling pathway, and within signalling pathways in general, is the presence of multiple feedforward and feedback loops that are simultaneously activated. The interactions between these subnetworks through their kinetics and the strength of their regulatory impact on the broader network is not well understood. For example, we discovered that MYC2 and MYC3 stimulate JA biosynthesis and target the entire JAZ repressor family from which the majority of members are also transcriptionally activated. Uncoupling these subnetworks would be an effective way to determine how they interact to drive very robust activation of the JA pathway. The combination of our multi-omics framework approach coupled with powerful genetic approaches, such as the generation of the *jaz* decuple mutant[29], should significantly contribute to a better understanding of JA response pathways.

Methods

Plant material and growth conditions. The *myc2* mutant *jin1-8* (SALK_061267)[15] was obtained from the Arabidopsis Biological Resource Center. Col-0 *MYC2::MYC2-YPet* and Col-0 *MYC3::MYC3-YPet*, generated by recombineering, have been previously described[67]. For the generation of all large-scale datasets, 3-day-old etiolated seedlings were used (Col-0 (WT), *myc2*, *MYC2::MYC2-YPet* and *MYC3::MYC3-YPet*). Seedlings were grown in the dark in closed lightproof containers. Gaseous methyl jasmonate treatments for the respective times were performed in these containers, as previously described[17], with 1 µl of methyl jasmonate (95% purity; Sigma-Aldrich) per 1 litre of container volume dropped onto Whatman paper. For the JA-induced root-growth inhibition assay, surface-sterilized WT, *myc2* and T-DNA mutant seeds (Supplementary Table 19) were grown on agar plates containing Linsmaier and Skoog (LS) medium supplemented with or without 20 µM methyl jasmonate (392707, Millipore Sigma) for 9 days. Plates were scanned afterwards and root lengths were measured using ImageJ.

ChIP-seq. Three-day-old etiolated Col-0 *MYC2::MYC2-YPet*, Col-0 *MYC3::MYC3-YPet*, Col-0 and *myc2* seedlings were used for ChIP-seq experiments. ChIP assays were performed as previously described[68]. ChIP-seq assays were conducted with antibodies against H2A.Z (39647, Active Motif), H3K4me3 (04–745, Millipore Sigma) and green fluorescent protein (GFP; 11814460001, Millipore Sigma or goat anti-GFP supplied by D. Dreschel, Max Planck Institute of Molecular Cell Biology and Genetics). As a negative control, mouse or goat IgG (015–000–003 or 005–000–003, Jackson ImmunoResearch) was used. The respective antibodies or IgG were coupled for 4–6 h to Protein G Dynabeads (50 µl, 10004D, Thermo Fisher Scientific) and subsequently incubated overnight with equal amounts of sonicated chromatin. Beads were washed twice with high-salt buffer (50 mM Tris-HCl pH 7.4, 150 mM NaCl, 2 mM EDTA, 0.5% Triton X-100), low-salt buffer (50 mM Tris-HCl pH 7.4, 500 mM NaCl, 2 mM EDTA, 0.5% Triton X-100) and wash buffer (50 mM Tris-HCl pH 7.4, 50 mM NaCl, 2 mM EDTA) before samples were decrosslinked, digested with proteinase K and DNA precipitated. Sequencing libraries were generated following the manufacturer's instructions (Illumina). Libraries were sequenced on a Illumina HiSeq 2500 and HiSeq 4000 Sequencing system, and sequencing reads were aligned to the TAIR10 genome assembly using Bowtie2 (ref. [69]).

DAP-seq. DAP-seq assays were carried out as previously described[70,71] using recombinantly expressed ERF1, ORA59, ATAF1 (also known as AT1G01720), DREB2B, ZAT18, RVE2, WRKY51, HY5 and TCP23.

RNA-seq. Three-day-old etiolated seedlings were used for expression analyses. Total RNA was extracted using a RNeasy Plant Mini kit (74903, Qiagen). Complementary DNA library preparation and subsequent single-read sequencing were carried as previously described[3].

RNA-seq analyses. Sequencing reads were quality trimmed using TrimGalore 0.4.5 (https://github.com/FelixKrueger/TrimGalore) then aligned to the TAIR10 genome assembly using TopHat 2.1.1 (ref. [72]). Reads within gene models were counted using HTSeq[73]. Differentially expressed genes in time-series RNA-seq were identified using EdgeR 3.6.2 with a likelihood ratio test (using the functions glmFit and glmLRT), and batch correction using Benjamini–Hochberg correction was used for multiple tests[74]. Differentially expressed genes in the Col-0 versus *myc2* mutant RNA-seq were determined using EdgeR 3.18.1 and quasi-likelihood *F*-tests (using the function glmQLFit)[75]. Temporal co-regulation of transcripts was determined using Short Time-Series Expression Miner (STEM)[76]. A minimum correlation coefficient of 0.7 was applied, and up to 50 permutations were permitted to identify correct cluster/gene matches. Significant clusters were those having a Bonferroni-corrected $P < 0.05$. Full STEM model parameters are given in Supplementary Table 7. Known *A. thaliana* TFs were identified by reference to PlantTFDB 4.0 (ref. [77]).

ChIP-seq and DAP-seq analyses. ChIP-seq and DAP-seq sequence reads were mapped to the TAIR10 reference genome using Bowtie2 v.2–2.0.5 with default parameters[78]. For TF and histone ChIP-seq, we first assessed the quality of the ChIP data by using PhantomPeakQualTools v.2.0 to calculate normalized strand correlation, relative strand correlation and shift size[79]. Enriched binding sites were then identified using MACS2 v.2.1 (options -p 99e-2–nomodel –shiftsize–down-sample–call-summits) against sequence reads from whole IgG control samples[80]. Subsequent analyses used summits only. Summit lists were filtered with a cut-off of $P \leq 1 \times 10^{-25}$, and remaining summits expanded from single nucleotides to 150 nt. Only summits with at least 10% nucleotide overlap between at least two biological replicates were retained. These overlapping summits were merged between replicates using BEDtools v.2.17.0 to give the final set of high-confidence binding sites, which were then annotated using ChIPpeakAnno v.2.2.0 to any gene within 500 nt of the centre of the summit or, alternatively, the nearest neighbour if there was no gene within 500 nt[81,82]. Venn diagrams were drawn using Venny and Intervene (http://bioinfogp.cnb.csic.es/tools/venny/)[83]. Top-ranked MYC2 and MYC3 binding sites were identified by applying irreproducible discovery rate to the summits from the two biological replicates that had the greatest number of summits above the MACS2 cut-off of $P \leq 1 \times 10^{-25}$. TF binding motifs were determined using the MEME-ChIP webserver with default parameters on the sequences of the high-stringency MYC2 summits[84]. To identify potential partner TFs that may enable indirect MYC2 binding, we removed all MYC2 high-stringency summits that contained the MYC2 motif (CACGTG, CATGTG or CACGTT). This was done by scanning them with FIMO set to default parameters (http://meme-suite.org/tools/fimo) against the position weight matrix for the MYC2 motif we previously identified by MEME-ChIP. We then conducted MEME-ChIP analyses on the remaining high-stringency summits as described above.

The Genome wide Event finding and Motif discovery (GEM) tool[85] was used to identify the target summits in DAP-seq data. Significant enrichments of histone modifications and histone variants were identified with the software SICER[86] using the TAIR10 genome assembly. The Intersect tool from BEDtools[81] was used to identify the genes in the histone ChIP-seq datasets most proximal to the binding sites. The fraction of reads in peak score was calculated for DAP-seq and histone ChIP-seq data using BEDtools and SAMtools[86,87]. For both ChIP-seq and DAP-seq, GO enrichment was assessed using clusterProfiler with default parameters[88]. Protein domain enrichment was assessed using Thalemine (https://apps.araport.org/thalemine/) with default parameters[89].

Mass spectrometry analysis. Untreated and JA-treated Col-0 and *myc2* seedling tissue samples were ground and lysed in YeastBuster (71186, Millipore Sigma). Proteins (100 µg per sample) were precipitated using methanol–chloroform. Dried pellets were dissolved in 8 M urea, 100 mM triethylammonium bicarbonate (TEAB), reduced with 5 mM Tris (2-carboxyethyl) phosphine hydrochloride (TCEP) and alkylated with 50 mM chloroacetamide. Proteins were then trypsin digested overnight at 37 °C. The digested peptides were labelled using a TMT10plex Isobaric Label Reagent set (90309, Thermo Fisher Scientific, lot no. TE264412) and combined. One hundred micrograms (the pre-enriched sample) was fractionated using a basic reverse-phase kit (84868, Thermo Fisher Scientific). Phospho-peptides were enriched from the remaining sample (900 µg) using a High-Select Fe-NTA Phospho-peptide Enrichment kit (A32992, Thermo Fisher Scientific). The TMT labelled samples were analysed on a Fusion Lumos mass spectrometer (Thermo Fisher Scientific). Samples were injected directly onto a 25 cm, 100-µm inner diameter column packed with BEH 1.7-µm C18 resin (186002350, Waters) and subsequently separated at a flow rate of 300 nl min^{-1} on a nLC 1200 (LC140, Thermo Fisher Scientific). Buffer A and B were 0.1% formic acid in water and 90% acetonitrile, respectively. A gradient of 1–20% B over 180 min, an increase to 40% B over 30 min, an increase to 100% B over another 20 min and held at 90% B for a final 10 min of washing was used for a total run time of 240 min. The column was re-equilibrated with 20 µl of buffer A before the injection of sample. Peptides were eluted directly from the tip of the column and nano sprayed directly into the mass spectrometer by application of 2.8 kV voltage at the back of the column. The Lumos was operated in the data-dependent mode. Full MS1 scans were collected in the Orbitrap at 120,000 resolution. The cycle time was set to 3 s, and within this 3 s, the most abundant ions per scan were selected for tandem mass spectrometry with collision-induced dissociation in the ion trap. MS3 analysis with multinotch isolation (SPS3) was utilized for detection of TMT reporter ions at 60,000 resolution. Monoisotopic precursor selection was enabled and dynamic exclusion was used with an exclusion duration of 10 s.

The raw data were analysed using MaxQuant (v.1.6.3.3)[90]. Spectra were searched using the Andromeda search engine[91] against the TAIR10 proteome file entitled "TAIR10_pep_20101214" that was downloaded from the TAIR website (https://www.arabidopsis.org/download/indexauto.jsp?dir=%2Fdownload_files%2FProteins%2FTAIR10_protein_lists) and was complemented with reverse decoy sequences and common contaminants by MaxQuant. Carbamidomethyl cysteine was set as a fixed modification, while methionine oxidation and protein amino-terminal acetylation were set as variable modifications. For the phoshoproteome, "Phosho STY" was also set as a variable modification. The sample type was set to "Reporter Ion MS3" with "10plex TMT selected for both lysine and N-termini". Digestion parameters were set to "specific" and "Trypsin/P;LysC". Up to two missed cleavages were allowed. A FDR, calculated in MaxQuant using a target-decoy strategy[92], value of less than 0.01 at both the peptide spectral match and protein identification level was required. The 'second peptide' option to identify co-fragmented peptides was not used. Differentially expressed proteins and phospho-sites were identified using PoissonSeq[93] with a *q*-value cut-off of 0.1. Sample loading normalization was performed before differential expression analysis.

Transcript quantification and identification of isoform switches. Quantification of transcripts was performed using Salmon v.0.8.1 in conjunction with the AtRTD2-QUASI transcript reference[94,95]. The quasi mapping-based index was built using an auxiliary *k*-mer hash over *k*-mers of length 31 ($k=31$). For quantification, all parameters of Salmon were kept at default; however, the option to correct for the fragment-level GC biases ("–gcBias") was turned on. The TSIS R package[96], which is designed for detecting alternatively spliced isoform-switch events in time-series transcriptome data, was used to perform the isoform-switch analysis. Only transcripts whose average TPM across all time points was >1 were included in the TSIS analysis. The mean expression approach was used to search interaction points. Significant switch events were identified using the following filtering parameters: (1) probability cut-off value of >0.5; (2) differences cut-off value of >1; (3) *P* cut-off value of <0.05; (4) minimum time in interval of >1.

Gene regulatory network inference. All gene regulatory network inferences were constructed using the Regression Tree Pipeline for Spatial, Temporal, and Replicate data (RTP-STAR)[97,98]. Before gene regulatory network inference, genes were clustered on the basis of transcriptome, proteome or phosphoproteome data using Dynamic Time Warping and the dtwclust package in R[99]. These clusters were then used in the RTP-STAR pipeline. For the transcriptome networks, one network was inferred for genes differentially expressed at each time point (eight networks in total), and then the networks were combined in a union. For each network, the biological replicates for that individual time point and the 0 h (control) time point were used to infer the network. The sign (activation/repression) of each edge was inferred using all of the time points in the time course. For the proteome and phosphoproteome networks, one network was inferred for genes differentially expressed in any of the comparisons. The biological replicates for all of the (phospho)proteome samples were used to infer the network. The sign of each edge was not inferred, as the (phospho)proteome data only consisted of one time point. After the transcriptome, proteome and phosphoproteome networks were combined in a union, a Network Motif Score (NMS)[100] was calculated to determine the importance of each gene. Feedback loop, feedforward loop, bi-fan and diamond motifs were used in this score as they have been previously shown to contain genes important for biological processes[101–103]. All motifs that were significantly enriched in the combined network were compared to a randomly generated network of the same size. The number of times each gene appeared in each motif was counted, the counts were normalized to a scale of 0 to 1, and the counts were summed to calculate the NMS. The higher the NMS, the more functionally important the gene. All code for RTP-STAR is available at https://github.com/nmclark2/RTP-STAR. The parameters used for all networks in this paper are provided in Supplementary Table 20.

Reporting Summary. Further information on research design is available in the Nature Research Reporting Summary linked to this article.

Data availability

All described lines can be requested from the corresponding authors. Sequence data can be downloaded from the Gene Expression Omnibus repository (GSE133408). Proteomics data are deposited at the ProteomeXchange under the accession ID PXD013592. Visualized data can be found at http://neomorph.salk.edu/MYC2 and http://signal.salk.edu/interactome/JA.php. Source data for Figs. 1–5 and Extended Data Figs. 1–10 are provided with the paper.

Received: 5 August 2019; Accepted: 23 January 2020;
Published online: 13 March 2020

References

1. Vanstraelen, M. & Benkova, E. Hormonal interactions in the regulation of plant development. *Annu. Rev. Cell Dev. Biol.* **28**, 463–487 (2012).
2. Chang, K. N. et al. Temporal transcriptional response to ethylene gas drives growth hormone cross-regulation in *Arabidopsis*. *eLife* **2**, e00675 (2013).
3. Song, L. et al. A transcription factor hierarchy defines an environmental stress response network. *Science* **354**, aag1550 (2016).
4. Hickman, R. et al. Architecture and dynamics of the jasmonic acid gene regulatory network. *Plant Cell* **29**, 2086–2105 (2017).
5. Pauwels, L. et al. Mapping methyl jasmonate-mediated transcriptional reprogramming of metabolism and cell cycle progression in cultured *Arabidopsis* cells. *Proc. Natl Acad. Sci. USA* **105**, 1380–1385 (2008).
6. Wang, C., Liu, Y., Li, S. S. & Han, G. Z. Insights into the origin and evolution of the plant hormone signaling machinery. *Plant Physiol.* **167**, 872–886 (2015).
7. Huang, H., Liu, B., Liu, L. & Song, S. Jasmonate action in plant growth and development. *J. Exp. Bot.* **68**, 1349–1359 (2017).
8. Thines, B. et al. JAZ repressor proteins are targets of the SCF(COI1) complex during jasmonate signalling. *Nature* **448**, 661–665 (2007).
9. Chini, A. et al. The JAZ family of repressors is the missing link in jasmonate signalling. *Nature* **448**, 666–671 (2007).
10. Fonseca, S. et al. (+)-7-*iso*-Jasmonoyl-L-isoleucine is the endogenous bioactive jasmonate. *Nat. Chem. Biol.* **5**, 344–350 (2009).
11. Sheard, L. B. et al. Jasmonate perception by inositol-phosphate-potentiated COI1–JAZ co-receptor. *Nature* **468**, 400–405 (2010).
12. Xie, D. X. et al. *COI1*: an *Arabidopsis* gene required for jasmonate-regulated defense and fertility. *Science* **280**, 1091–1094 (1998).
13. Fernandez-Calvo, P. et al. The *Arabidopsis* bHLH transcription factors MYC3 and MYC4 are targets of JAZ repressors and act additively with MYC2 in the activation of jasmonate responses. *Plant Cell* **23**, 701–715 (2011).
14. Song, S. et al. MYC5 is involved in jasmonate-regulated plant growth, leaf senescence and defense responses. *Plant Cell Physiol.* **58**, 1752–1763 (2017).
15. Lorenzo, O., Chico, J. M., Sanchez-Serrano, J. J. & Solano, R. *JASMONATE-INSENSITIVE1* encodes a MYC transcription factor essential to discriminate between different jasmonate-regulated defense responses in *Arabidopsis*. *Plant Cell* **16**, 1938–1950 (2004).
16. Zhang, F. et al. Structural basis of JAZ repression of MYC transcription factors in jasmonate signalling. *Nature* **525**, 269–273 (2015).
17. Schweizer, F. et al. *Arabidopsis* basic helix–loop–helix transcription factors MYC2, MYC3, and MYC4 regulate glucosinolate biosynthesis, insect performance, and feeding behavior. *Plant Cell* **25**, 3117–3132 (2013).

18. Bao, S. et al. Molecular basis of natural variation in photoperiodic flowering responses. *Dev. Cell* **50**, 90–101 (2019).
19. Du, M. et al. MYC2 orchestrates a hierarchical transcriptional cascade that regulates jasmonate-mediated plant immunity in tomato. *Plant Cell* **29**, 1883–1906 (2017).
20. Dombrecht, B. et al. MYC2 differentially modulates diverse jasmonate-dependent functions in *Arabidopsis*. *Plant Cell* **19**, 2225–2245 (2007).
21. Yadav, V. et al. A basic helix–loop–helix transcription factor in *Arabidopsis*, MYC2, acts as a repressor of blue light-mediated photomorphogenic growth. *Plant Cell* **17**, 1953–1966 (2005).
22. Gangappa, S. N. & Chattopadhyay, S. MYC2, a bHLH transcription factor, modulates the adult phenotype of SPA1. *Plant Signal. Behav.* **5**, 1650–1652 (2010).
23. Zhang, X. et al. Jasmonate-activated MYC2 represses ETHYLENE INSENSITIVE3 activity to antagonize ethylene-promoted apical hook formation in *Arabidopsis*. *Plant Cell* **26**, 1105–1117 (2014).
24. Gimenez-Ibanez, S. et al. JAZ2 controls stomata dynamics during bacterial invasion. *New Phytol.* **213**, 1378–1392 (2017).
25. Fernandez, P. C. et al. Genomic targets of the human c-Myc protein. *Genes Dev.* **17**, 1115–1129 (2003).
26. Godoy, M. et al. Improved protein-binding microarrays for the identification of DNA-binding specificities of transcription factors. *Plant J.* **66**, 700–711 (2011).
27. Xie, M. et al. A B-ARR-mediated cytokinin transcriptional network directs hormone cross-regulation and shoot development. *Nat. Commun.* **9**, 1604 (2018).
28. Liu, Y. et al. MYC2 regulates the termination of jasmonate signaling via an autoregulatory negative feedback loop. *Plant Cell* **31**, 106–127 (2019).
29. Guo, Q. et al. JAZ repressors of metabolic defense promote growth and reproductive fitness in *Arabidopsis*. *Proc. Natl Acad. Sci. USA* **115**, E10768–E10777 (2018).
30. Pauwels, L. et al. NINJA connects the co-repressor TOPLESS to jasmonate signalling. *Nature* **464**, 788–791 (2010).
31. Huot, B., Yao, J., Montgomery, B. L. & He, S. Y. Growth-defense tradeoffs in plants: a balancing act to optimize fitness. *Mol. Plant* **7**, 1267–1287 (2014).
32. Chen, X. et al. New perspective of the bHLH–MYB complex in jasmonate-regulated plant fertility in *Arabidopsis*. *Plant Signal. Behav.* **11**, e1135280 (2016).
33. Hou, X. et al. DELLAs modulate jasmonate signaling via competitive binding to JAZs. *Dev. Cell* **19**, 884–894 (2010).
34. Lorenzo, O., Piqueras, R., Sanchez-Serrano, J. J. & Solano, R. ETHYLENE RESPONSE FACTOR1 integrates signals from ethylene and jasmonate pathways in plant defense. *Plant Cell* **15**, 165–178 (2003).
35. Pre, M. et al. The AP2/ERF domain transcription factor ORA59 integrates jasmonic acid and ethylene signals in plant defense. *Plant Physiol.* **147**, 1347–1357 (2008).
36. Bu, Q. et al. Role of the *Arabidopsis thaliana* NAC transcription factors ANAC019 and ANAC055 in regulating jasmonic acid-signaled defense responses. *Cell Res.* **18**, 756–767 (2008).
37. Gao, Q. M., Venugopal, S., Navarre, D. & Kachroo, A. Low oleic acid-derived repression of jasmonic acid-inducible defense responses requires the WRKY50 and WRKY51 proteins. *Plant Physiol.* **155**, 464–476 (2011).
38. Pauwels, L. & Goossens, A. Fine-tuning of early events in the jasmonate response. *Plant Signal. Behav.* **3**, 846–847 (2008).
39. Schweizer, F. et al. Differential contribution of transcription factors to *Arabidopsis thaliana* defense against *Spodoptera littoralis*. *Front. Plant. Sci.* **4**, 13 (2013).
40. Taki, N. et al. 12-Oxo-phytodienoic acid triggers expression of a distinct set of genes and plays a role in wound-induced gene expression in *Arabidopsis*. *Plant Physiol.* **139**, 1268–1283 (2005).
41. Xiao, J., Jin, R. & Wagner, D. Developmental transitions: integrating environmental cues with hormonal signaling in the chromatin landscape in plants. *Genome Biol.* **18**, 88 (2017).
42. Wang, H. et al. MED25 connects enhancer-promoter looping and MYC2-dependent activation of jasmonate signalling. *Nat. Plants* **5**, 616–625 (2019).
43. Rothbart, S. B. & Strahl, B. D. Interpreting the language of histone and DNA modifications. *Biochim. Biophys. Acta* **1839**, 627–643 (2014).
44. Coleman-Derr, D. & Zilberman, D. Deposition of histone variant H2A.Z within gene bodies regulates responsive genes. *PLoS Genet.* **8**, e1002988 (2012).
45. Kawaguchi, R. & Bailey-Serres, J. mRNA sequence features that contribute to translational regulation in *Arabidopsis*. *Nucleic Acids Res.* **33**, 955–965 (2005).
46. Walley, J. W. et al. Integration of omic networks in a developmental atlas of maize. *Science* **353**, 814–818 (2016).
47. Hartmann, L. et al. Alternative splicing substantially diversifies the transcriptome during early photomorphogenesis and correlates with the energy availability in *Arabidopsis*. *Plant Cell* **28**, 2715–2734 (2016).
48. Chung, H. S. et al. Alternative splicing expands the repertoire of dominant JAZ repressors of jasmonate signaling. *Plant J.* **63**, 613–622 (2010).
49. Moreno, J. E. et al. Negative feedback control of jasmonate signaling by an alternative splice variant of JAZ10. *Plant Physiol.* **162**, 1006–1017 (2013).
50. Nakata, M. et al. A bHLH-type transcription factor, ABA-INDUCIBLE BHLH-TYPE TRANSCRIPTION FACTOR/JA-ASSOCIATED MYC2-LIKE1, acts as a repressor to negatively regulate jasmonate signaling in *Arabidopsis*. *Plant Cell* **25**, 1641–1656 (2013).
51. Sasaki-Sekimoto, Y. et al. Basic helix–loop–helix transcription factors JASMONATE-ASSOCIATED MYC2-LIKE1 (JAM1), JAM2, and JAM3 are negative regulators of jasmonate responses in *Arabidopsis*. *Plant Physiol.* **163**, 291–304 (2013).
52. Xu, J. et al. Activation of MAPK kinase 9 induces ethylene and camalexin biosynthesis and enhances sensitivity to salt stress in *Arabidopsis*. *J. Biol. Chem.* **283**, 26996–27006 (2008).
53. Hentrich, M. et al. The jasmonic acid signaling pathway is linked to auxin homeostasis through the modulation of YUCCA8 and YUCCA9 gene expression. *Plant J.* **74**, 626–637 (2013).
54. Wild, M. et al. The *Arabidopsis* DELLA RGA-LIKE3 is a direct target of MYC2 and modulates jasmonate signaling responses. *Plant Cell* **24**, 3307–3319 (2012).
55. Mittler, R. et al. Gain- and loss-of-function mutations in *Zat10* enhance the tolerance of plants to abiotic stress. *FEBS Lett.* **580**, 6537–6542 (2006).
56. Lozano-Duran, R. et al. The transcriptional regulator BZR1 mediates trade-off between plant innate immunity and growth. *eLife* **2**, e00983 (2013).
57. Magome, H. et al. The DDF1 transcriptional activator upregulates expression of a gibberellin-deactivating gene, *GA2ox7*, under high-salinity stress in *Arabidopsis*. *Plant J.* **56**, 613–626 (2008).
58. Dubois, M. et al. The ETHYLENE RESPONSE FACTORs ERF6 and ERF11 antagonistically regulate mannitol-induced growth inhibition in *Arabidopsis*. *Plant Physiol.* **169**, 166–179 (2015).
59. Zander, M. et al. Repression of the *Arabidopsis thaliana* jasmonic acid/ethylene-induced defense pathway by TGA-interacting glutaredoxins depends on their C-terminal ALWL motif. *Mol. Plant* **5**, 831–840 (2012).
60. Ndamukong, I. et al. SA-inducible *Arabidopsis* glutaredoxin interacts with TGA factors and suppresses JA-responsive PDF1.2 transcription. *Plant J.* **50**, 128–139 (2007).
61. Shyu, C. et al. JAZ8 lacks a canonical degron and has an EAR motif that mediates transcriptional repression of jasmonate responses in *Arabidopsis*. *Plant Cell* **24**, 536–550 (2012).
62. Ren, X. et al. ABO3, a WRKY transcription factor, mediates plant responses to abscisic acid and drought tolerance in *Arabidopsis*. *Plant J.* **63**, 417–429 (2010).
63. Alonso, J. M. Genome-wide insertional mutagenesis of *Arabidopsis thaliana*. *Science* **301**, 653–657 (2003).
64. Arabidopsis Genome Initiative. Analysis of the genome sequence of the flowering plant *Arabidopsis thaliana*. *Nature* **408**, 796–815 (2000).
65. Huang, J., Ghosh, R. & Bankaitis, V. A. Sec14-like phosphatidylinositol transfer proteins and the biological landscape of phosphoinositide signaling in plants. *Biochim. Biophys. Acta* **1861**, 1352–1364 (2016).
66. Mosblech, A. et al. Jasmonic acid perception by COI1 involves inositol polyphosphates in *Arabidopsis thaliana*. *Plant J.* **65**, 949–957 (2011).
67. Zhou, R., Benavente, L. M., Stepanova, A. N. & Alonso, J. M. A recombineering-based gene tagging system for *Arabidopsis*. *Plant J.* **66**, 712–723 (2011).
68. Kaufmann, K. et al. Chromatin immunoprecipitation (ChIP) of plant transcription factors followed by sequencing (ChIP-SEQ) or hybridization to whole genome arrays (ChIP–CHIP). *Nat. Protoc.* **5**, 457–472 (2010).
69. Langmead, B. Aligning short sequencing reads with Bowtie. *Curr. Protoc. Bioinformatics* **Chapter 11**, Unit 11 17 (2010).
70. O'Malley, R. C. et al. Cistrome and epicistrome features shape the regulatory DNA landscape. *Cell* **165**, 1280–1292 (2016).
71. Bartlett, A. et al. Mapping genome-wide transcription-factor binding sites using DAP-seq. *Nat. Protoc.* **12**, 1659–1672 (2017).
72. Kim, D. et al. TopHat2: accurate alignment of transcriptomes in the presence of insertions, deletions and gene fusions. *Genome Biol.* **14**, R36 (2013).
73. Anders, S., Pyl, P. T. & Huber, W. HTSeq—a Python framework to work with high-throughput sequencing data. *Bioinformatics* **31**, 166–169 (2015).
74. Robinson, M. D., McCarthy, D. J. & Smyth, G. K. edgeR: a Bioconductor package for differential expression analysis of digital gene expression data. *Bioinformatics* **26**, 139–140 (2010).
75. Lun, A. T., Chen, Y. & Smyth, G. K. It's DE-licious: a recipe for differential expression analyses of RNA-seq experiments using quasi-likelihood methods in edgeR. *Methods Mol. Biol.* **1418**, 391–416 (2016).
76. Ernst, J. & Bar-Joseph, Z. STEM: a tool for the analysis of short time series gene expression data. *BMC Bioinformatics* **7**, 191 (2006).
77. Jin, J. et al. PlantTFDB 4.0: toward a central hub for transcription factors and regulatory interactions in plants. *Nucleic Acids Res.* **45**, D1040–D1045 (2017).

78. Langmead, B. & Salzberg, S. L. Fast gapped-read alignment with Bowtie 2. *Nat. Methods* **9**, 357–359 (2012).
79. Kharchenko, P. V., Tolstorukov, M. Y. & Park, P. J. Design and analysis of ChIP-seq experiments for DNA-binding proteins. *Nat. Biotechnol.* **26**, 1351–1359 (2008).
80. Zhang, Y. et al. Model-based analysis of ChIP-Seq (MACS). *Genome Biol.* **9**, R137 (2008).
81. Quinlan, A. R. & Hall, I. M. BEDTools: a flexible suite of utilities for comparing genomic features. *Bioinformatics* **26**, 841–842 (2010).
82. Zhu, L. J. et al. ChIPpeakAnno: a Bioconductor package to annotate ChIP-seq and ChIP-chip data. *BMC Bioinformatics* **11**, 237 (2010).
83. Khan, A. & Mathelier, A. Intervene: a tool for intersection and visualization of multiple gene or genomic region sets. *BMC Bioinformatics* **18**, 287 (2017).
84. Machanick, P. & Bailey, T. L. MEME-ChIP: motif analysis of large DNA datasets. *Bioinformatics* **27**, 1696–1697 (2011).
85. Guo, Y., Mahony, S. & Gifford, D. K. High resolution genome wide binding event finding and motif discovery reveals transcription factor spatial binding constraints. *PLoS Comput. Biol.* **8**, e1002638 (2012).
86. Zang, C. et al. A clustering approach for identification of enriched domains from histone modification ChIP-Seq data. *Bioinformatics* **25**, 1952–1958 (2009).
87. Li, H. et al. The sequence alignment/map format and SAMtools. *Bioinformatics* **25**, 2078–2079 (2009).
88. Yu, G., Wang, L. G., Han, Y. & He, Q.-Y. clusterProfiler: an R package for comparing biological themes among gene clusters. *Omics* **16**, 284–287 (2012).
89. Krishnakumar, V. et al. Araport: the *Arabidopsis* information portal. *Nucleic Acids Res.* **43**, D1003–D1009 (2015).
90. Tyanova, S., Temu, T. & Cox, J. The MaxQuant computational platform for mass spectrometry-based shotgun proteomics. *Nat. Protoc.* **11**, 2301–2319 (2016).
91. Cox, J. et al. Andromeda: a peptide search engine integrated into the MaxQuant environment. *J. Proteome Res.* **10**, 1794–1805 (2011).
92. Elias, J. E. & Gygi, S. P. Target-decoy search strategy for mass spectrometry-based proteomics. *Methods Mol. Biol.* **604**, 55–71 (2010).
93. Li, J., Witten, D. M., Johnstone, I. M. & Tibshirani, R. Normalization, testing, and false discovery rate estimation for RNA-sequencing data. *Biostatistics* **13**, 523–538 (2012).
94. Patro, R. et al. Salmon provides fast and bias-aware quantification of transcript expression. *Nat. Methods* **14**, 417–419 (2017).
95. Zhang, R. et al. AtRTD—a comprehensive reference transcript dataset resource for accurate quantification of transcript-specific expression in *Arabidopsis thaliana*. *New Phytol.* **208**, 96–101 (2015).
96. Guo, W., Calixto, C. P. G., Brown, J. W. S. & Zhang, R. TSIS: an R package to infer alternative splicing isoform switches for time-series data. *Bioinformatics* **33**, 3308–3310 (2017).
97. Shibata, M. et al. GTL1 and DF1 regulate root hair growth through transcriptional repression of *ROOT HAIR DEFECTIVE 6-LIKE 4* in *Arabidopsis*. *Development* **145**, dev159707 (2018).
98. Clark, N. M. et al. Auxin induces widespread proteome remodeling in *Arabidopsis* seedlings. *Proteomics* **19**, e1900199 (2019).
99. Giorgino, T. Computing and visualizing dynamic time warping alignments in R: the dtw package. *J. Stat. Softw.* https://doi.org/10.18637/jss.v031.i07 (2012).
100. Clark, N. M. et al. Stem-cell-ubiquitous genes spatiotemporally coordinate division through regulation of stem-cell-specific gene networks. *Nat. Commun.* **10**, 5574 (2019).
101. Alon, U. Network motifs: theory and experimental approaches. *Nat. Rev. Genet.* **8**, 450–461 (2007).
102. Milo, R. et al. Network motifs: simple building blocks of complex networks. *Science* **298**, 824–827 (2002).
103. Ingram, P. J., Stumpf, M. P. & Stark, J. Network motifs: structure does not determine function. *BMC Genomics* **7**, 108 (2006).

Acknowledgements

M.Z. was supported by a Deutsche Forschungsgemeinschaft (DFG) research fellowship (Za-730/1-1) and by the Salk Pioneer Postdoctoral Endowment Fund. M.G.L. was supported by an EU Marie Curie FP7 International Outgoing Fellowship (252475). In addition, this work was supported by the Mass Spectrometry Core of the Salk Institute with funding from NIH-NCI CCSG (P30 014195) and the Helmsley Center for Genomic Medicine. This work was supported by grants from the National Science Foundation (NSF) (MCB-1818160 and IOS-1759023 to J.W.W., MCB-1024999 to J.R.E.), the National Institutes of Health (R01GM120316), the Division of Chemical Sciences, Geosciences, and Biosciences, the Office of Basic Energy Sciences of the US Department of Energy (DE-FG02-04ER15517), and the Gordon and Betty Moore Foundation (GBMF3034). Research in the lab of R.S. was supported by grant BIO2016-77216-R (MINECO/FEDER) from the Ministry of Economy, Industry and Competitiveness. J.W.W. is supported as a Faculty Scholar of the ISU Plant Sciences Institute. J.R.E. is an Investigator of the Howard Hughes Medical Institute. We thank the following postdocs, undergraduates and technicians who contributed technical assistance to the project: M. Xie, L. Song, R. Carlos Serrano, C. Sy, L. Tames, J. Park, O. Romero, R. Luong, W. Ho, Y. Koga, S. Hazelton, M. Urich and T. Dabi. We thank S.-s. C. Huang for computational assistance and J. Moresco and J. Diedrich for proteomics support.

Author contributions

M.Z., M.G.L., R.S. and J.R.E. designed the research. M.Z., M.G.L., A.E.L. and B.J. performed the phenotype screening. M.Z., M.G.L. and J.P.S.G. carried out the RNA-seq and ChIP-seq experiments. M.G.L., E.H. and J.P.S.G. performed the cloning and generation of transgenic constructs. M.G.L., J.R.N., H.C., M.Z. and L.Y. analysed the sequencing data and performed bioinformatics analyses. A.B. carried out DAP-seq experiments. N.M.C. and J.W.W. analysed the proteome and phosphoproteome data. N.M.C., J.W.W., A.W. and Z.B.-J. performed regulatory network analyses. M.Z., M.G.L. and J.R.E. prepared the figures and wrote the manuscript.

Competing interests

The authors declare no competing interests.

Additional information

Extended data is available for this paper at https://doi.org/10.1038/s41477-020-0605-7.

Supplementary information is available for this paper at https://doi.org/10.1038/s41477-020-0605-7.

Correspondence and requests for materials should be addressed to M.G.L. or J.R.E.

Peer review information *Nature Plants* thanks Pingtao Ding, Jonathan Jones, Chuanyou Li and the other, anonymous, reviewer for their contribution to the peer review of this work.

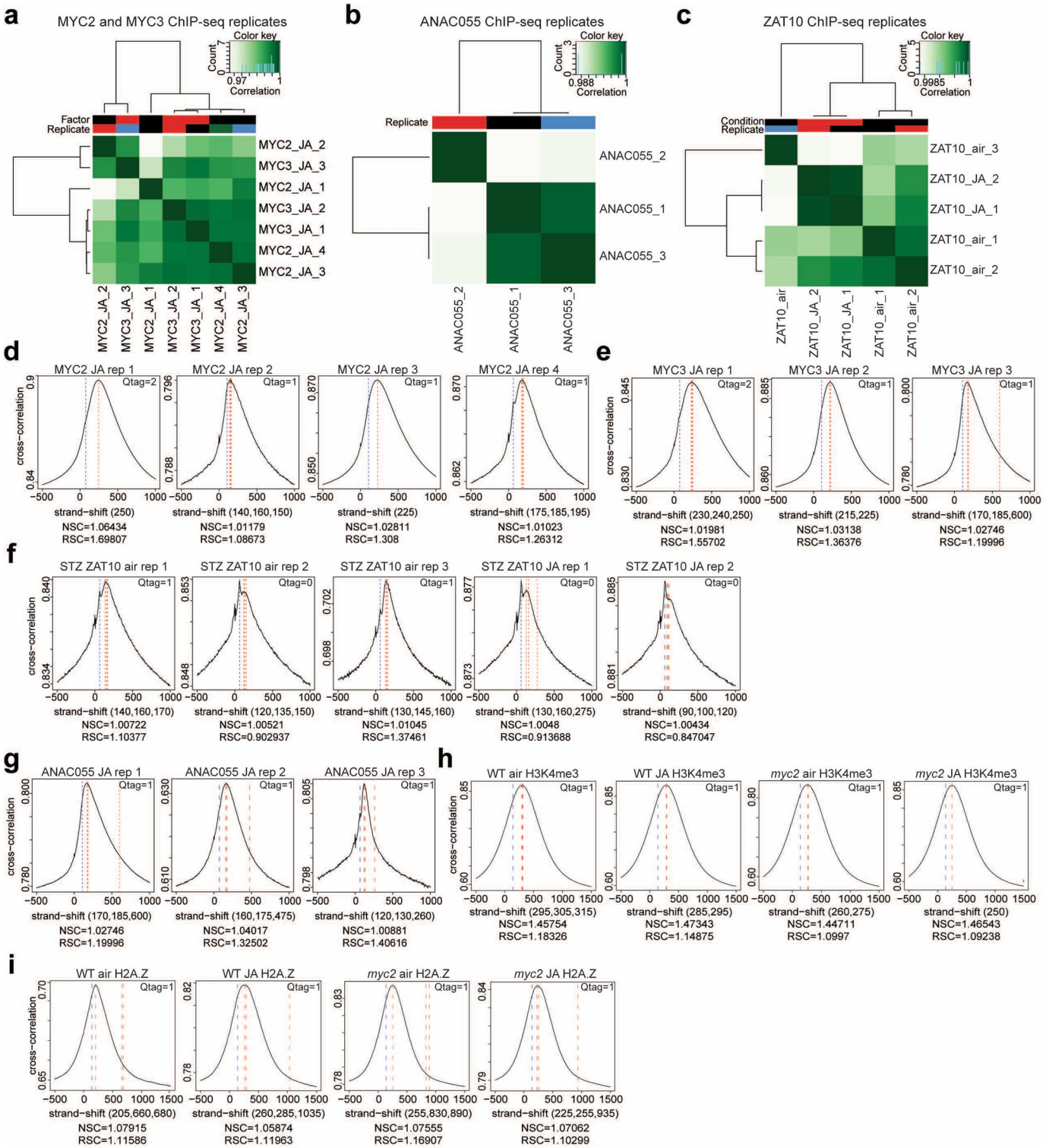

Extended Data Fig. 1 | Overview of quality metrics of generated ChIP-seq datasets. a–c, Correlation plot of the respective TF ChIP-seq samples is shown. The MYC2 and MYC3 ChIP-seq replicates are shown together in (**a**). Clustering is determined by the degree of correlation (Pearson correlation). ChIP-seq data is derived from at least three independent experiments: MYC2 (JA, n = 4), MYC3 (JA, n = 3), ZAT10 (air, n = 3; JA, n = 2), ANAC055 (JA, n = 3). d-i, Cross-correlation (Pearson correlation) plot for the respective TF and histone ChIP-Seq sample is shown. NSC means normalized strand cross-correlation coefficient and RSC means relative strand cross-correlation coefficient. Qtag means quality tag based on thresholded RSC (codes = −2: very low, −1: low, 0: medium, 1: high, 2: very high). All shown TF ChIP-seq replicates are derived from independent experiments: MYC2 (JA, n = 4), MYC3 (JA, n = 3), ZAT10 (air, n = 3; JA, n = 2), ANAC055 (JA, n = 3). Histone ChIP-seq data is derived from a single experiment (n = 1).

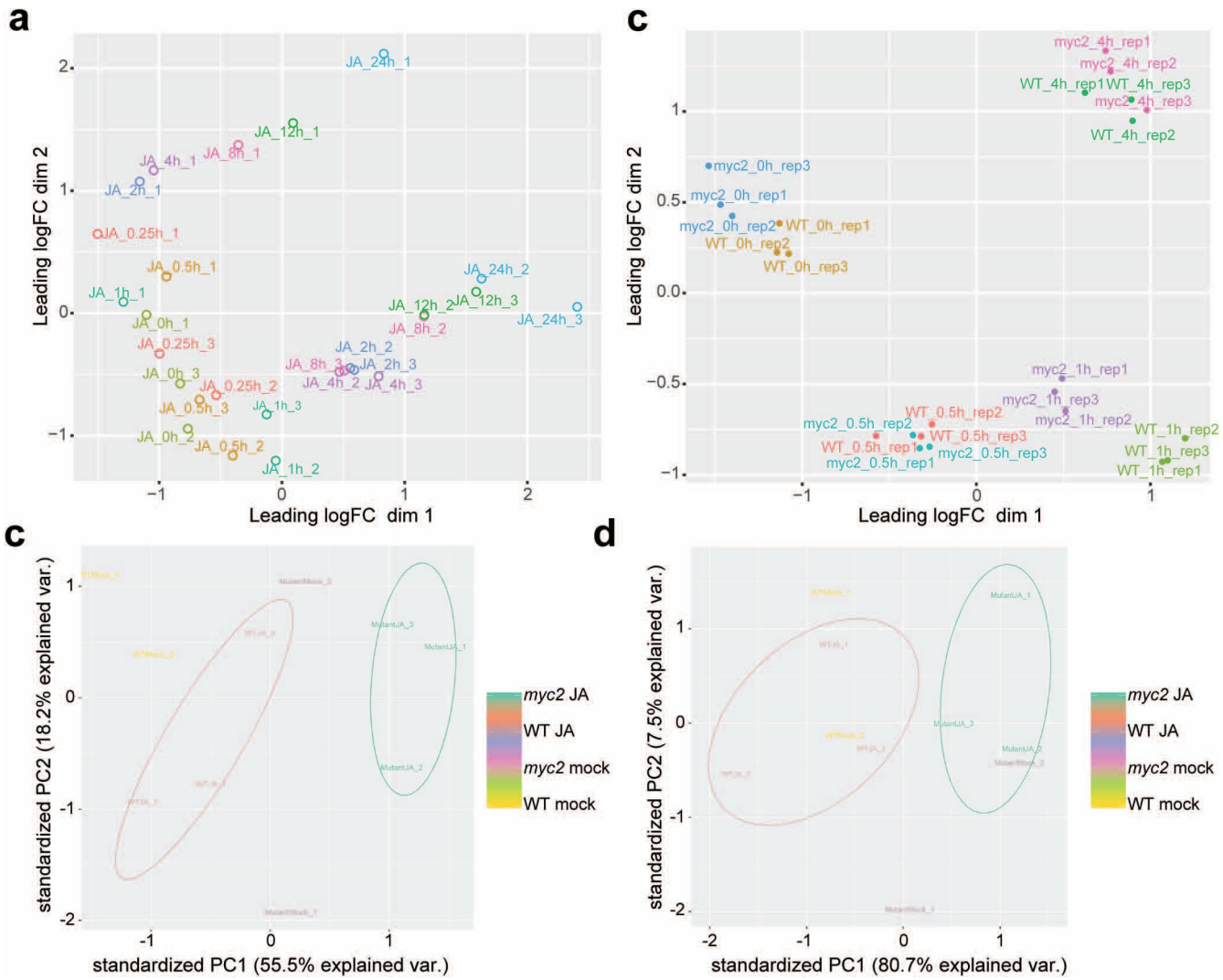

Extended Data Fig. 2 | Overview of quality metrics of generated RNA-seq and proteome data. a,**b**, Multidimensional scaling (MDS) plots of replicate samples of the 24 h JA treatment RNA-seq time-series in WT (**a**) and the 4 h JA-treatment RNA-seq time-series in WT and *myc2* seedlings (**b**) are shown. Both JA treatment time series consist of three independent samples (n = 3) for each time point and genotype. c, d, Principal component analysis (PCA) plots of independent biological replicate samples analyzed by proteomics (**c**) and phosphoproteomics (**d**).

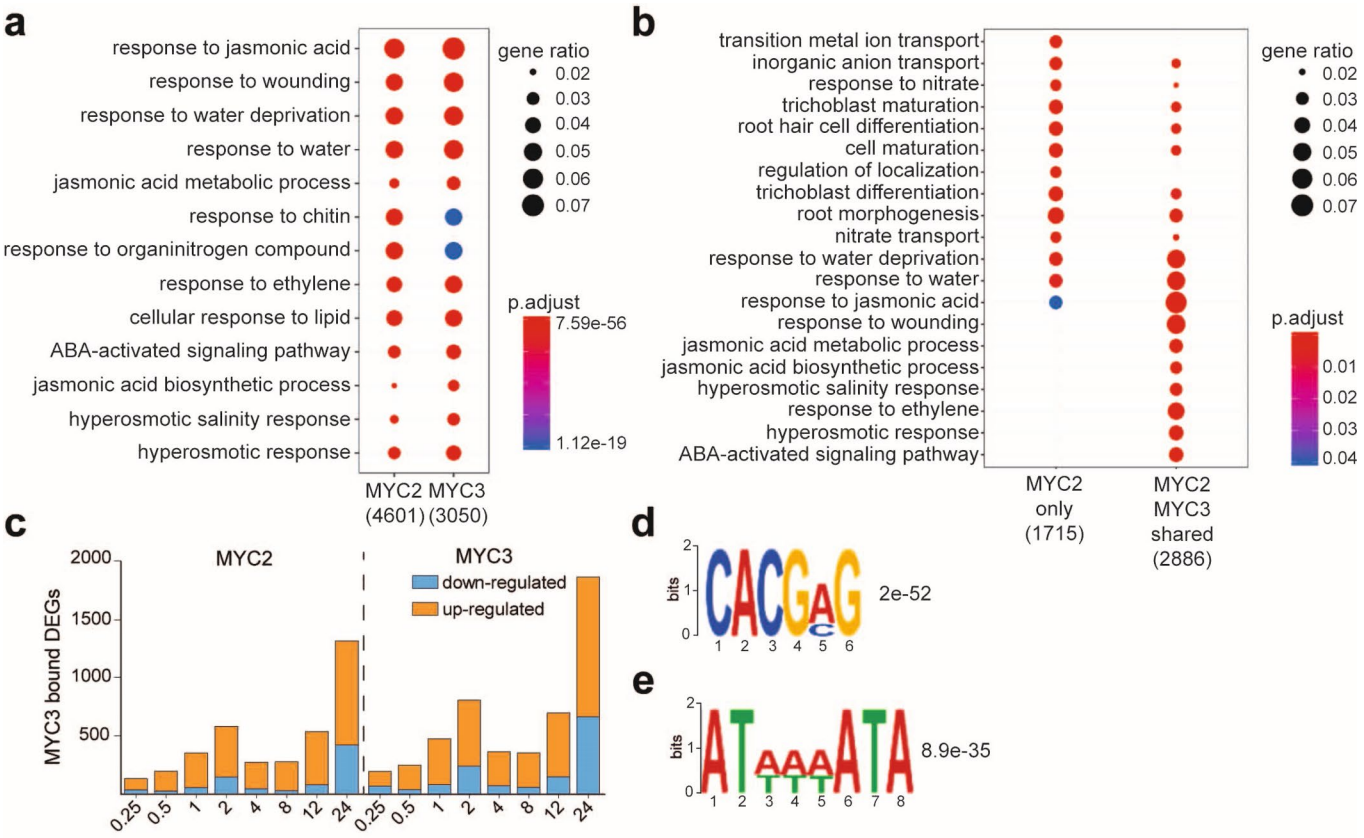

Extended Data Fig. 3 | MYC2 and MYC3 act predominantly as activators for a functionally diverse range of target genes. a,**b**, Gene ontology (GO) analyses using a hypergeometric distribution of all MYC2 and MYC3 targets (**a**) as well as MYC2 only and MYC2/MYC3 shared targets (**b**) are shown. Data is derived from four independent MYC2 (n = 4) and three independent MYC3 (n = 3) ChIP-seq samples. Analyses were conducted using clusterProfiler. c, Bar plots shows the portion of JA-induced and JA-repressed genes that are bound by MYC2 and MYC3. **d**, **e**, The CACG[A/C]G motif (286 sites, $E = 2*10^{-52}$) (**d**) and the AT[A/T][A/T] [A/T]ATA motif (714 sites, $E = 8.9*10^{-35}$) (**e**) were enriched in MYC2 high-confidence target regions that do not contain a G-box or the degenerate G-box motifs CATGTG or CACGTT.

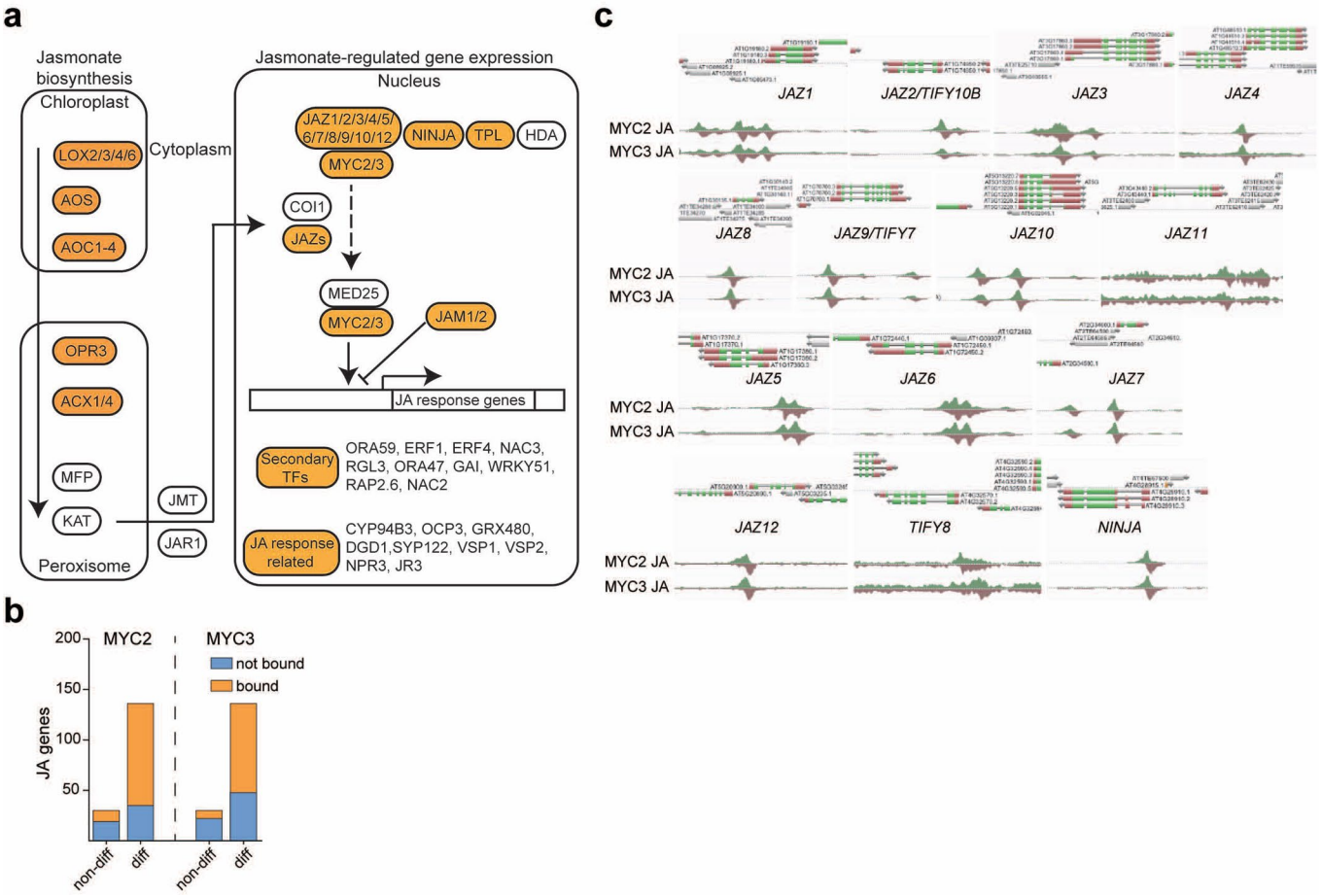

Extended Data Fig. 4 | MYC2 and MYC3 regulate the majority of JA signaling pathway components. a, Schematic overview of known MYC2/MYC3-targeted JA pathway components. Genes that are directly targeted by MYC2/MYC3 are highlighted in orange. **b**, Binding behavior of MYC2 and MYC3 at known JA genes (Supplementary Table 6) is shown. Known JA genes are grouped into non-differentially expressed and JA differentially expressed genes. **c**, AnnoJ genome browser screenshot visualizes MYC2 and MYC3 binding at all 13.

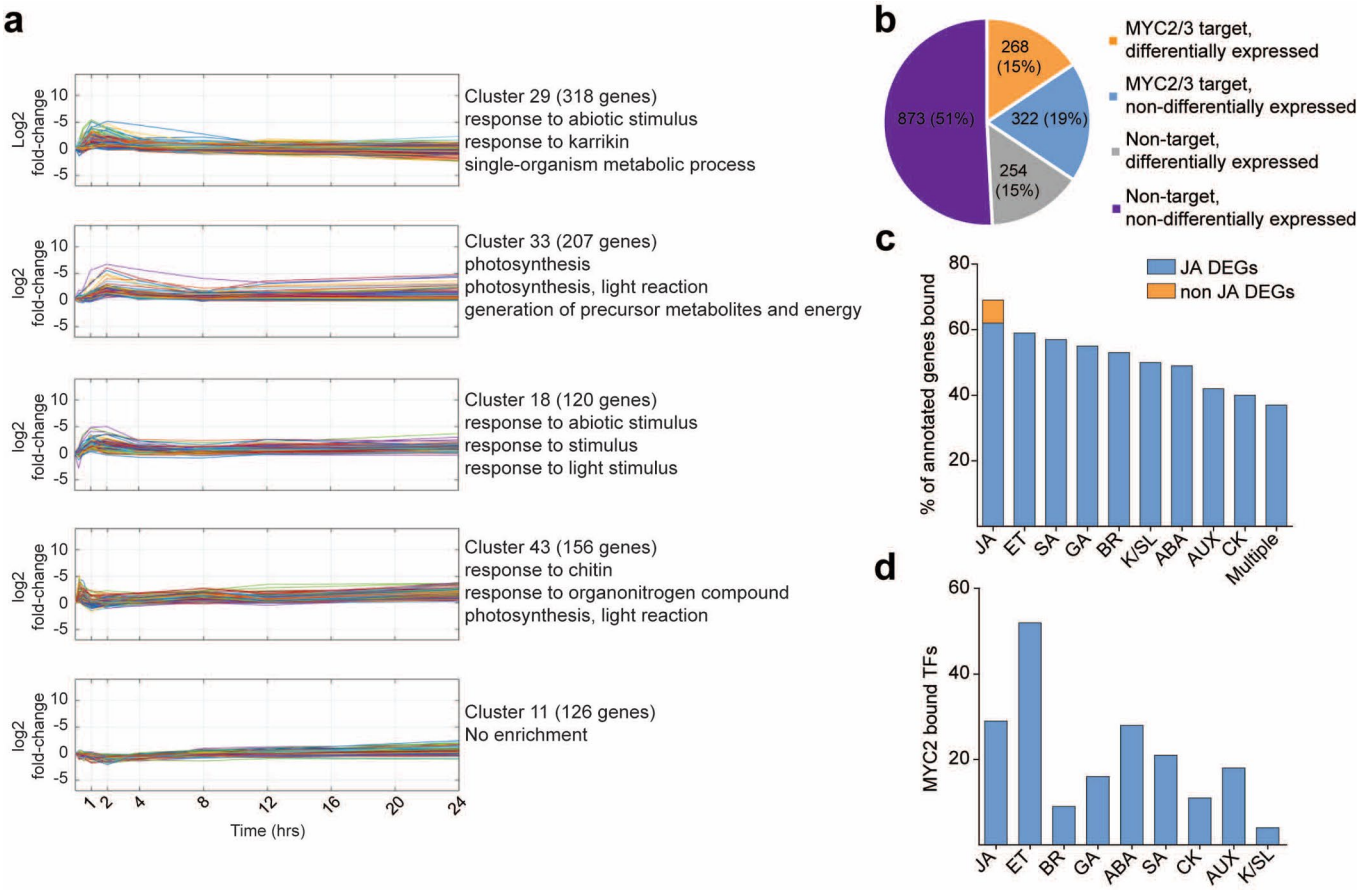

Extended Data Fig. 5 | MYC2 and MYC3 target a large number of TFs. a. Cluster analysis revealed the 5 other main clusters in the JA time course experiment. Clusters visualize the log2 fold change expression dynamics over the indicated 24 hours' time period. The three strongest enriched gene ontology terms for each cluster are shown as well. **b**, Pie chart indicates the proportions of TFs that are transcriptionally induced by JA, bound by MYC2/MYC3, or both. **c**,**d**, Overview of MYC2/MYC3-bound plant hormone genes (**c**) and TFs (**d**) is shown. Plant hormones are abbreviated (ET (ethylene), BR (brassinosteroids), GA (gibberellic acid), ABA (abscisic acid), SA (salicylic acid), CK (cytokinin), AUX (Auxin), K (karrikin), SL (strigolactones)).

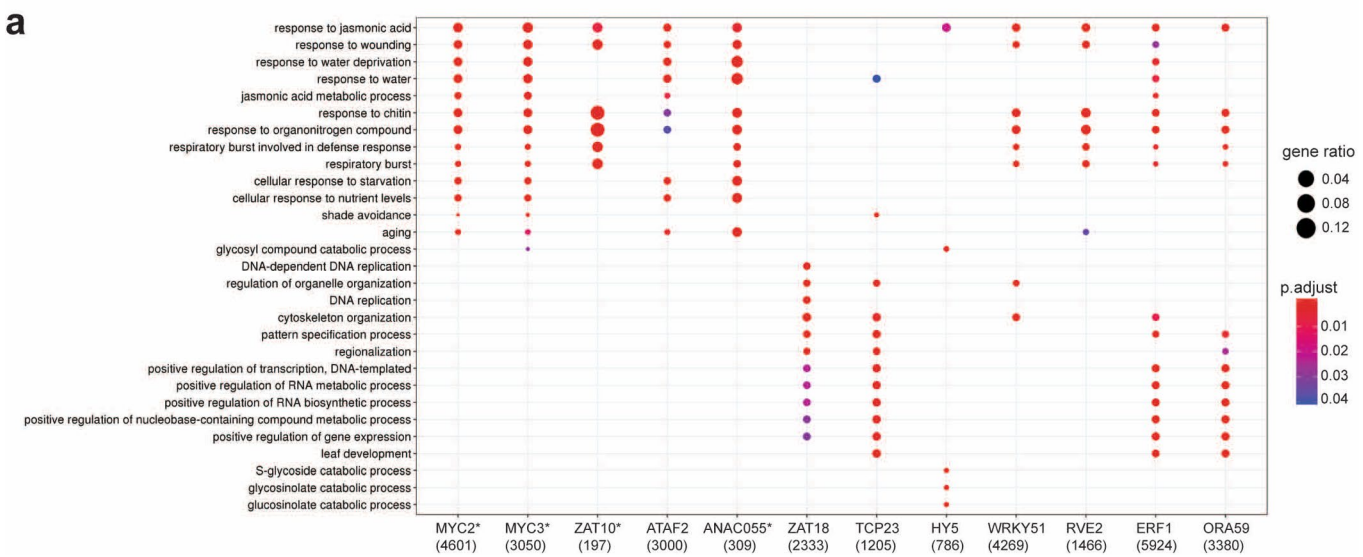

Extended Data Fig. 6 | Overview of MYC-controlled TF network. a. Significantly enriched (adjusted $p < 0.05$) gene ontology terms amongst the target of each TF. For each TF the 4 terms with the lowest p-value are shown, some of which are redundant between TFs. No enriched terms were detected for DREB2B targets. ChIP-seq data is indicated by presence of *, all other data was generated by DAP-seq. ChIP-seq data is derived from at least three independent experiments: MYC2 (JA, n = 4), MYC3 (JA, n = 3), ZAT10 (air, n = 3; JA, n = 2), ANAC055 (JA, n = 3). DAP-seq data is derived from a single experiment (n = 1).

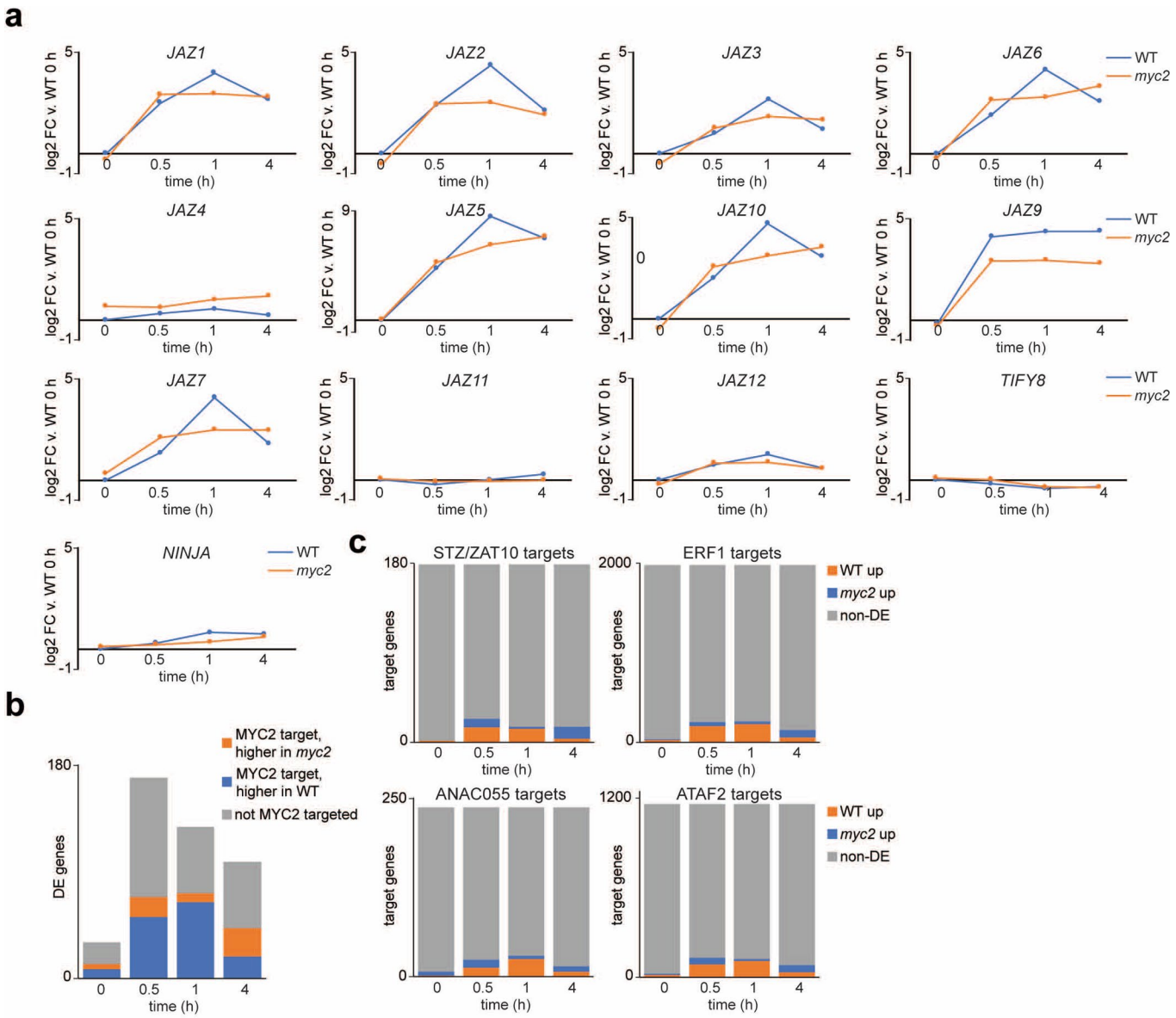

Extended Data Fig. 7 | MYC2 partially controls expression of JAZ repressors. a, Individual plots show expression of all *JAZ/TIFYs* and *NINJA* in WT (blue) and *myc2* (orange) seedlings following JA treatment. log2 fold change (FC) was calculated relative to their respective 0 h (ie. non-treated) control samples. **b**, Bar chart shows the number of differentially expressed (DE) genes at each time point after JA treatment between WT and *myc2* seedlings. The bar chart also indicates how many of these DE genes were direct binding targets of MYC2 (in ChIP-seq assays) and whether they were more highly expressed in WT (blue) or *myc2* (orange) seedlings. **c**, Charts indicates of how MYC2 indirectly affects the expression of downstream genes through secondary TFs. The expression of genes in pairwise comparisons of WT and *myc2* transcriptomes at 0, 0.5, 1 and 4 h was assessed. Only genes that were direct targets of the TFs ATAF2, ZAT10, ANACO55 and ERF1, and not direct targets of MYC2, were analyzed which are termed "non-MYC2 target genes". ATAF2, ZAT10, ANACO55 and ERF1 are themselves direct targets of MYC2 and their expression levels were decreased in *myc2* relative to WT, indicating they are directly regulated by MYC2. DE indicates differentially expressed genes.

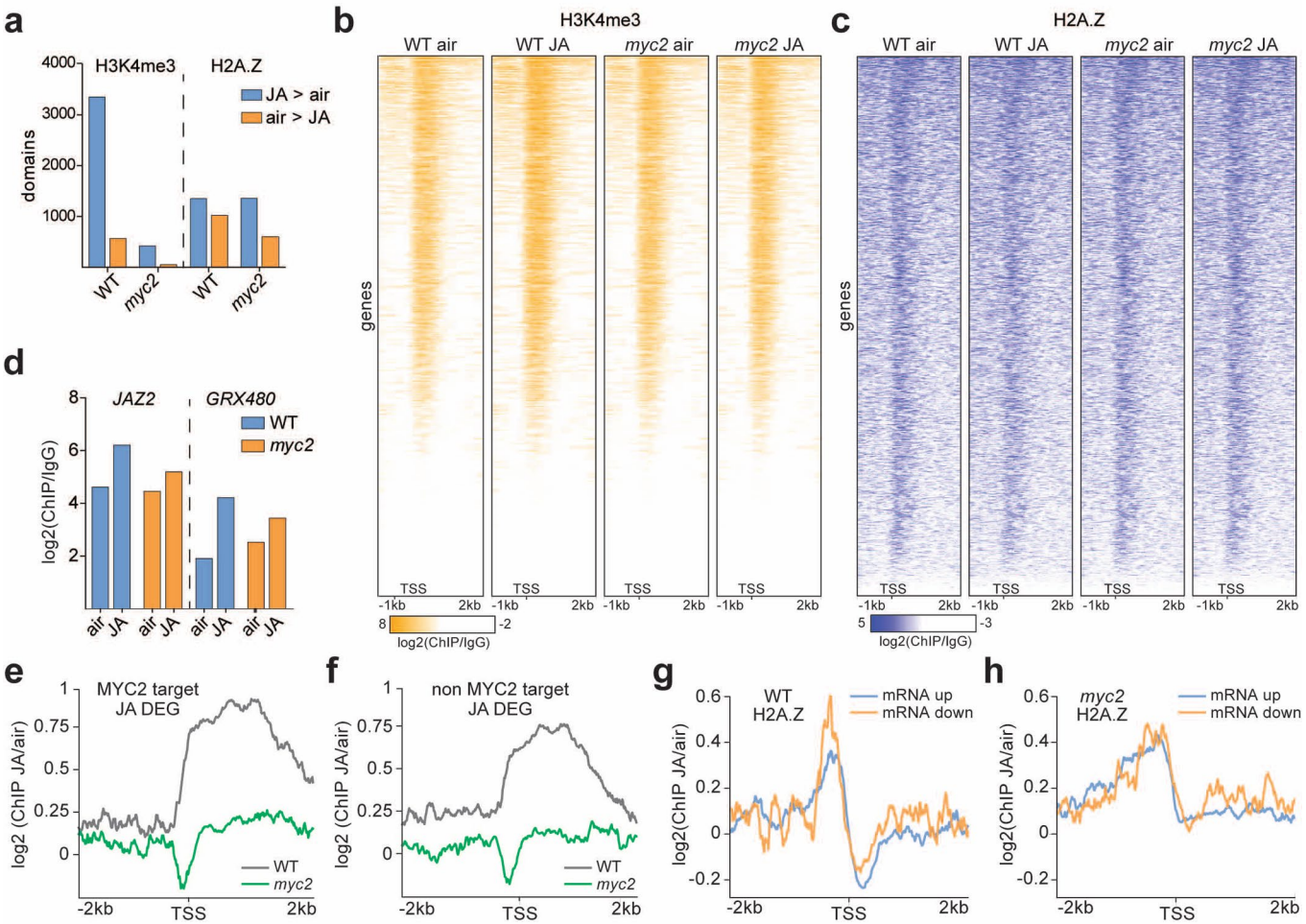

Extended Data Fig. 8 | JA shapes the local chromatin architecture. a, Bar plot shows the impact of two hours JA treatment on the genome-wide distribution of H3K4me3 and H2A.Z domains. Occupancy was determined in untreated/JA-treated WT and *myc2* seedlings using ChIP-seq. SICER was used to identify the number of histone domains that show an increase (blue) or decrease (orange) of enrichment in response to JA. **b**,**c**, Heatmaps show the occupancy of H3K4me3 and H2A.Z from 1 kb upstream to 2 kb downstream of the transcriptional start site (TSS) at all *Arabidopsis* genes (TAIR10). Heatmaps are shown for H3K4me3 (**b**) and H2A.Z (**c**) in untreated and JA-treated (4 h) WT and *myc2* seedlings. **d**, Quantification of H3K4me3 occupancy at *JAZ2* and *GRX480* is shown. It was calculated as the ratio between the respective ChIP-seq sample and the WT IgG control. **e**,**f**, Aggregated profiles show the $\log_2$ fold change enrichment of H3K4me3 at JA DEGs that are directly (**e**) and not directly targeted (**f**) by MYC2 from 2 kb upstream to 2 kb downstream of the transcriptional start site (TSS). **g**,**h**, Plot profiles show the $\log_2$ fold change enrichment of H2A.Z in WT (**g**) and *myc2* mutants (**h**) from 2 kb upstream to 2 kb downstream of the transcriptional start site (TSS) at JA-induced and JA-repressed genes.

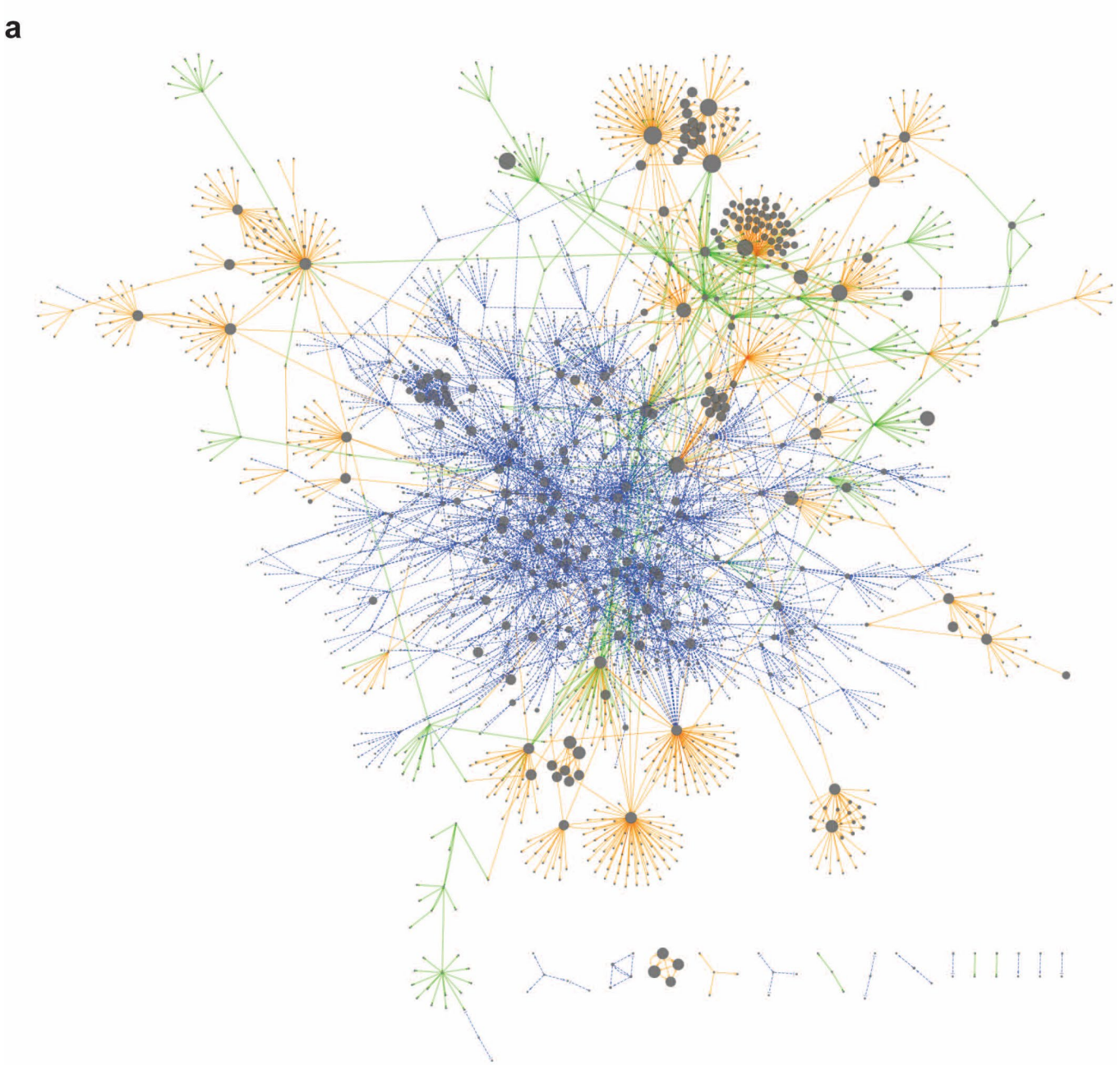

Extended Data Fig. 9 | The JA gene regulatory network. a, Illustration of JA gene regulatory network for 1, 2 and 4 h time points. Edges were predicted using phosphoproteome (green), proteome (orange) and transcriptome (blue) data. Node sizes are scaled by normalized motif score, with larger nodes indicating greater scores and likely greater importance within the network. Edges predicted early in the time-series transcriptomic data are red (0.25–2 h), edges predicted late are blue (4–24 h). Proteome and phosphoproteome-data-predicted edges are grey and green, respectively.

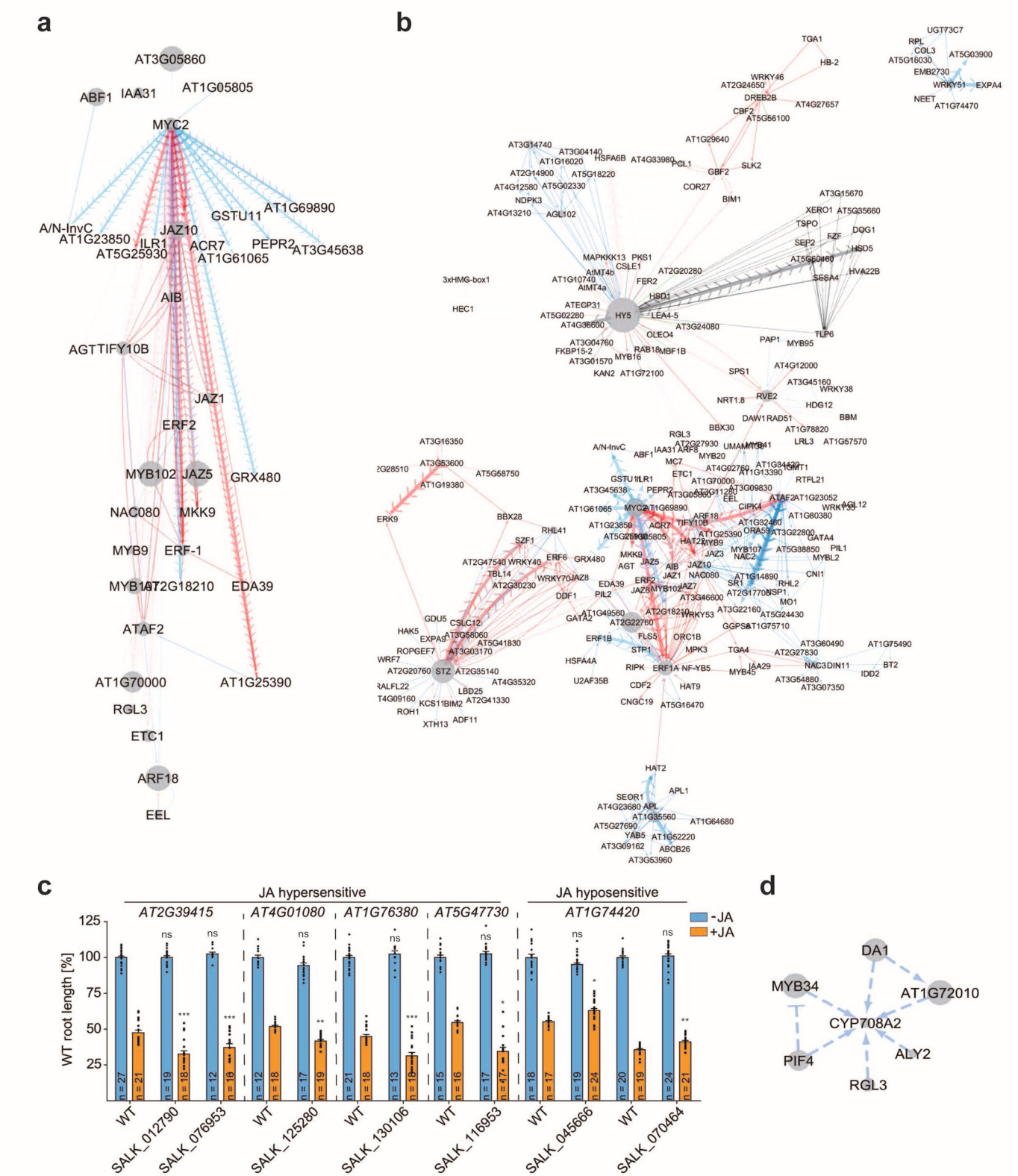

Extended Data Fig. 10 | Gene regulatory network validation against ChIP/DAP-seq data. a, The MYC2 subnetwork is shown. Edges are directional and red edges exist at early time points (0.25–2 h), blue only at late time points (4–24 h). Thicker edges with chevrons indicate that MYC2 were directly bound to that gene in our ChIP-seq experiments. **b**, Validated edges are those between TFs and first neighbors in the JA gene regulatory network for which the first neighbor was also a direct target of the TF in ChIP/DAP-seq assays. These edges are indicated by chevrons. Early time-series transcriptome-predicted edges (0.25–2 h) are red and later edges (4–24 h) are blue. Edges detected in the proteomic data are grey and those detected in the phosphoproteomic data are green. **c**, Bar plot shows quantification of JA-induced root growth inhibition in the indicated T-DNA alleles. Seedlings were grown on LS media with or without 20 μM MeJA. WT seedlings serve as independent controls for each tested T-DNA line. Sample size number n is shown within the respective bars. Samples are derived from three independent experiments. Asterisks represent significant differences between WT (-/+JA) and indicated T-DNA lines (-/+JA) (two-way ANOVA with Bonferroni post test, ns (not significant) $p > 0.05$, *$p < 0.05$, **$p < 0.01$, ***$p < 0.001$). **d**, Subnetwork of CYP708A2 is shown.

nature research

Corresponding author(s): Joseph R. Ecker, Mathew G. Lewsey

Last updated by author(s): Jan 14, 2020

Reporting Summary

Nature Research wishes to improve the reproducibility of the work that we publish. This form provides structure for consistency and transparency in reporting. For further information on Nature Research policies, see Authors & Referees and the Editorial Policy Checklist.

Statistics

For all statistical analyses, confirm that the following items are present in the figure legend, table legend, main text, or Methods section.

n/a	Confirmed
☐	☒ The exact sample size (*n*) for each experimental group/condition, given as a discrete number and unit of measurement
☒	☐ A statement on whether measurements were taken from distinct samples or whether the same sample was measured repeatedly
☐	☒ The statistical test(s) used AND whether they are one- or two-sided *Only common tests should be described solely by name; describe more complex techniques in the Methods section.*
☒	☐ A description of all covariates tested
☒	☐ A description of any assumptions or corrections, such as tests of normality and adjustment for multiple comparisons
☐	☒ A full description of the statistical parameters including central tendency (e.g. means) or other basic estimates (e.g. regression coefficient) AND variation (e.g. standard deviation) or associated estimates of uncertainty (e.g. confidence intervals)
☒	☐ For null hypothesis testing, the test statistic (e.g. *F*, *t*, *r*) with confidence intervals, effect sizes, degrees of freedom and *P* value noted *Give P values as exact values whenever suitable.*
☒	☐ For Bayesian analysis, information on the choice of priors and Markov chain Monte Carlo settings
☒	☐ For hierarchical and complex designs, identification of the appropriate level for tests and full reporting of outcomes
☒	☐ Estimates of effect sizes (e.g. Cohen's *d*, Pearson's *r*), indicating how they were calculated

Our web collection on statistics for biologists contains articles on many of the points above.

Software and code

Policy information about availability of computer code

Data collection	Sequencing data was generated and collected on the Illumina HiSeq 2500, HiSeq 4000 and MiSeq Sequencing systems. Proteomics data was collected on a Fusion Lumos mass spectrometer (Thermo Fisher Scientific). Root length was measured using ImageJ.
Data analysis	Genomics: TopHat 2.1.1, HTSeq, EdgeR 3.6.2, EdgeR 3.18.1, PlantTFDB 4.0, Bowtie 2 v.2-2.0.5, MACS2 v.2.1, PhantomPeakQualTools v.2.0, BEDtools v.2.17.0, ChIPpeakAnno v.2.2.0, SICER, BEDtools, clusterProfiler, Salmon v0.8.1, TSIS R package, SAMtools and Thalemine Proteomics: MaxQuant version 1.6.3.3, PoissonSeq Gene regulatory network (GRN) inference: RTP-STAR (https://github.com/nmclark2/RTP-STAR), Dynamic Time Warping (DTW)

For manuscripts utilizing custom algorithms or software that are central to the research but not yet described in published literature, software must be made available to editors/reviewers. We strongly encourage code deposition in a community repository (e.g. GitHub). See the Nature Research guidelines for submitting code & software for further information.

Data

Policy information about availability of data

All manuscripts must include a data availability statement. This statement should provide the following information, where applicable:

- Accession codes, unique identifiers, or web links for publicly available datasets
- A list of figures that have associated raw data
- A description of any restrictions on data availability

All described lines can be requested from the corresponding author. Sequence data can be downloaded from GEO (GSE133408, reviewer password 'efinoygcdbanzgh'). Proteomics data are deposited at Proteome Exchange under the accession ID PXD013592 (Reviewer Access: Username: "reviewer72788@ebi.ac.uk" and password: "Dwq1vRej"). Visualized sequencing data can be found under http://neomorph.salk.edu/MYC2.

Field-specific reporting

Please select the one below that is the best fit for your research. If you are not sure, read the appropriate sections before making your selection.

☒ Life sciences ☐ Behavioural & social sciences ☐ Ecological, evolutionary & environmental sciences

For a reference copy of the document with all sections, see nature.com/documents/nr-reporting-summary-flat.pdf

Life sciences study design

All studies must disclose on these points even when the disclosure is negative.

Sample size	The sample sizes in our study were chosen based on accepted sample sizes in relevant published reports within this field. (2-3 biological replicates for genomics and proteomic analyses were used).
Data exclusions	No data was excluded.
Replication	All of the experiments were repeated more than two times, and were reproduced successfully. A completely independent pool of side-by-side grown plants is considered as a biological replicate.
Randomization	Different genotypes were grown on individual plates and were allocated randomly in the growth and treatment chamber.
Blinding	Not applicable since no group allocation was conducted in this study.

Reporting for specific materials, systems and methods

We require information from authors about some types of materials, experimental systems and methods used in many studies. Here, indicate whether each material, system or method listed is relevant to your study. If you are not sure if a list item applies to your research, read the appropriate section before selecting a response.

Materials & experimental systems

n/a	Involved in the study
☐	☒ Antibodies
☒	☐ Eukaryotic cell lines
☒	☐ Palaeontology
☒	☐ Animals and other organisms
☒	☐ Human research participants
☒	☐ Clinical data

Methods

n/a	Involved in the study
☐	☒ ChIP-seq
☒	☐ Flow cytometry
☒	☐ MRI-based neuroimaging

Antibodies

Antibodies used	Htz1 / Histone H2A.Z antibody (pAb), Rabbit polyclonal (Active Motif Cat# 39647, RRID:AB_2793289), Lot 29018003, 10µl per reaction Anti-trimethyl-Histone H3 (Lys4), clone 15-10C-E4, Recombinant antibody, Rabbit monoclonal (Millipore Cat# 05-745R, RRID:AB_1587134), Lot 2420405, 4µl per reaction Anti-GFP antibody, Clones 7.1 and 13.1, Mouse monoclonal, (Sigma-Aldrich Cat# 11814460001, RRID:AB_390913), 5µl per reaction ChromPure Mouse IgG, whole molecule, Jackson ImmunoResearch, (Jackson ImmunoResearch Labs Cat# 015-000-003, RRID:AB_2337188), Lot 99413, 2µl per reaction goat anti-GFP supplied by David Dreschel, Max Planck Institute of Molecular Cell Biology and Genetics
Validation	All used antibodies were previously published in plant science-related studies (Htz1 / Histone H2A.Z antibody PMID:31418686), (Anti-trimethyl-Histone H3 (Lys4) PMID:31418686, PMID:30657772), anti-GFP PMID:28943086). Specificity of the Htz1 / Histone H2A.Z antibody was tested in Arabidopsis thaliana (PMID:31418686). The Anti-trimethyl-Histone H3 (Lys4) antibody has a broad species cross-reactivity expected and is used in various organism (PMID:30955888, PMID:24341414, PMID:22763441). Detailed antibody information can be found on the Antibody registry website (https://antibodyregistry.org) (Htz1 / Histone H2A.Z antibody, AB_2793289), (Anti-trimethyl-Histone H3 (Lys4), RRID:AB_1587134), (Anti-GFP antibody, RRID:AB_390913), (ChromPure Mouse IgG, RRID:AB_2337188).

ChIP-seq

Data deposition

☒ Confirm that both raw and final processed data have been deposited in a public database such as GEO.

☒ Confirm that you have deposited or provided access to graph files (e.g. BED files) for the called peaks.

Data access links *May remain private before publication.*	reviewer password 'efinoygcdbanzgh' for GEO deposition GSE133408
Files in database submission	ChIP-seq_Col-0_IgG.fastq.gz ChIP-seq_Col-0_air_H3K4me3.fastq.gz ChIP-seq_Col-0_4hJA_H3K4me3.fastq.gz ChIP-seq_myc2_air_H3K4me3.fastq.gz ChIP-seq_myc2_4hJA_H3K4me3.fastq.gz ChIP-seq_Col-0_air_H2A.Z.fastq.gz ChIP-seq_Col-0_4hJA_H2A.Z.fastq.gz ChIP-seq_myc2_air_H2A.Z.fastq.gz ChIP-seq_myc2_4hJA_H2A.Z.fastq.gz 110915_2-W200-G600-FDR0.01-islandfiltered-normalized.wig 110915_6-W200-G600-FDR0.01-islandfiltered-normalized.wig 110915_9-W200-G600-FDR0.01-islandfiltered-normalized.wig 110915_12-W200-G600-FDR0.01-islandfiltered-normalized.wig 110915_1-W200-G600-FDR0.01-islandfiltered-normalized.wig 110915_5-W200-G600-FDR0.01-islandfiltered-normalized.wig 110915_8-W200-G600-FDR0.01-islandfiltered-normalized.wig 110915_11-W200-G600-FDR0.01-islandfiltered-normalized.wig ANAC055_JA_2hr_ChIP_rep1.fastq.gz ANAC055_JA_2hr_ChIP_rep2.fastq.gz ANAC055_JA_2hr_ChIP_rep3.fastq.gz MYC2_JA_2hr_ChIP_rep1.fastq.gz MYC2_JA_2hr_ChIP_rep2.fastq.gz MYC2_JA_2hr_ChIP_rep3.fastq.gz MYC2_JA_2hr_ChIP_rep4.fastq.gz MYC3_JA_2hr_ChIP_rep1.fastq.gz MYC3_JA_2hr_ChIP_rep2.fastq.gz MYC3_JA_2hr_ChIP_rep3.fastq.gz STZ_AIR_2hr_ChIP_rep1.fastq.gz STZ_AIR_2hr_ChIP_rep2.fastq.gz STZ_AIR_2hr_ChIP_rep3.fastq.gz STZ_JA_2hr_ChIP_rep1.fastq.gz STZ_JA_2hr_ChIP_rep2.fastq.gz HAL_1205_controlreads.fastq.gz JONAS_2093_controlreads.fastq.gz MISEQ_5018_controlreads.fastq.gz JONAS_2096_controlreads_1.fastq.gz JONAS_2096_controlreads_2.fastq.gz HAL_1389_AT1G32640_JA_MGLCHIP16_3_150521_peaks.bed JONAS_2273_AT1G32640_JA_MGLCHIP34_151214_summits.bed JONAS_2273_AT1G32640_JA_MGLCHIP35_151214_summits.bed JONAS_2206_AT1G32640_JA_JS_ChIP_8_2014_04_16_summits.bed JONAS_2206_AT5G46760_JA_JS_ChIP_8_2014_04_16_summits.bed JONAS_2273_AT5G46760_JA_MGLCHIP34_151214_summits.bed JONAS_2273_AT5G46760_JA_MGLCHIP35_151214_summits.bed HAL_1422_AT1G27730_AIR_MGLCHIP38_160125_summits.bed HAL_1424_AT1G27730_AIR_MGLCHIP39_160315_summits.bed HAL_1424_AT1G27730_AIR_MGLCHIP41_160315_summits.bed HAL_1422_AT1G27730_JA_MGLCHIP38_160125_summits.bed HAL_1424_AT1G27730_JA_MGLCHIP39_160315_summits.bed JONAS_2257_AT3G15500_JA_MGLCHIP18_150608_summits.bed HAL_1422_AT3G15500_JA_MGLCHIP38_160125_summits.bed HAL_1424_AT3G15500_JA_MGLCHIP39_160315_summits.bed
Genome browser session (e.g. UCSC)	http://neomorph.salk.edu/MYC2

Methodology

Replicates	MYC2 ChIP-seq - 4 biological replicates MYC3 ChIP-seq - 3 biological replicates ANAC055 ChIP-seq - 3 biological replicates ZAT10 air ChIP-seq - 3 biological replicates

ZAT10 JA ChIP-seq - 2 biological replicates
H3K4me3 and H2A.Z ChIP-seq - 1 biological replicate

Sequencing depth

Listed by file below - total reads, uniquely mapped reads. All TF ChIP-seq samples were 100 bp single-read sequencing. Histone ChIP-seq samples were 130bp single-read sequencing.

ANAC055_JA_2hr_ChIP_rep1.fastq.gz 21579630 15584500
ANAC055_JA_2hr_ChIP_rep2.fastq.gz 10130742 7224047
ANAC055_JA_2hr_ChIP_rep3.fastq.gz 49536769 32819761
MYC2_JA_2hr_ChIP_rep1.fastq.gz 34003716 25391190
MYC2_JA_2hr_ChIP_rep2.fastq.gz 20608966 15047692
MYC2_JA_2hr_ChIP_rep3.fastq.gz 51803765 38110692
MYC2_JA_2hr_ChIP_rep4.fastq.gz 38302426 32517237
MYC3_JA_2hr_ChIP_rep1.fastq.gz 30218545 22198075
MYC3_JA_2hr_ChIP_rep2.fastq.gz 50956817 38186708
MYC3_JA_2hr_ChIP_rep3.fastq.gz 30155159 21448372
ZAT10_AIR_2hr_ChIP_rep1.fastq.gz 42120531 31505002
ZAT10_AIR_2hr_ChIP_rep2.fastq.gz 38712323 27326200
ZAT10_AIR_2hr_ChIP_rep3.fastq.gz 37810305 22967198
ZAT10_JA_2hr_ChIP_rep1.fastq.gz 55361855 39415920
ZAT10_JA_2hr_ChIP_rep2.fastq.gz 48383504 34173250
HAL_1205_controlreads.fastq.gz 40354104 27796842
JONAS_2093_controlreads.fastq.gz 9011923 4912769
MISEQ_5018_controlreads.fastq.gz 3767246 2642492
JONAS_2096_controlreads_1.fastq.gz 4000000 2699412
JONAS_2096_controlreads_2.fastq.gz 3011044 2033072
ChIP-seq_Col-0_IgG.fastq.gz 13651415
ChIP-seq_Col-0_air_H3K4me3.fastq.gz 18808057
ChIP-seq_Col-0_4hJA_H3K4me3.fastq.gz 24758457
ChIP-seq_myc2_air_H3K4me3.fastq.gz 17103736
ChIP-seq_myc2_4hJA_H3K4me3.fastq.gz 18261319
ChIP-seq_Col-0_air_H2A.Z.fastq.gz 20268643
ChIP-seq_Col-0_4hJA_H2A.Z.fastq.gz 19722520
ChIP-seq_myc2_air_H2A.Z.fastq.gz 26945152

Antibodies

Htz1 / Histone H2A.Z antibody (pAb), Rabbit polyclonal (Active Motif Cat# 39647, RRID:AB_2793289), Lot 29018003, 10µl per reaction
Anti-trimethyl-Histone H3 (Lys4), clone 15-10C-E4, Recombinant antibody, Rabbit monoclonal (Millipore Cat# 05-745R, RRID:AB_1587134), Lot 2420405, 4µl per reaction
Anti-GFP antibody, Clones 7.1 and 13.1, Mouse monoclonal, (Sigma-Aldrich Cat# 11814460001, RRID:AB_390913), 5µl per reaction
ChromPure Mouse IgG, whole molecule, Jackson ImmunoResearch, (Jackson ImmunoResearch Labs Cat# 015-000-003, RRID:AB_2337188), Lot 99413, 2µl per reaction
goat anti-GFP supplied by David Dreschel, Max Planck Institute of Molecular Cell Biology and Genetics

Peak calling parameters

For TF ChIP-seq, enriched binding sites were identified using MACS2 v.2.1 (options -p 99e-2 --nomodel –shiftsize --down-sample --call-summits) against sequence reads from whole IgG control samples (Zhang et al., 2008). The shift size was calculated using PhantomPeakQualTools v.2.0 (Kharchenko et al., 2008). Significant enrichments of histone modifications and histone variants were identified with the SICER software (Zang et al., 2009) using the TAIR10 genome assembly.

Data quality

Transcription factor summit lists were filtered with a lower cut-off of -log10(25) and remaining summits expanded from single nucleotides to 150 nt. Only summits with at least 10% nt overlap between at least two biological replicates were retained. These overlapping summits were merged between replicates using BEDtools v.2.17.0 to give the final set of high-stringency summits, which were then annotated using ChIPpeakAnno v.2.2.0 to any gene within 500 nt of the center of the summit or, alternatively, the nearest neighbor if there was no gene within 500 nt.

Software

Bowtie 2 v.2-2.0.5, MACS2 v.2.1, PhantomPeakQualTools v.2.0, BEDtools v.2.17.0, ChIPpeakAnno v.2.2.0, SICER